CMR-78-4

FINAL TECHNICAL REPORT

(LONG RANGE MATERIALS RESEARCH) DEVELOPMENT OF ELEVATED TEMPERATURE ELECTROCRYSTALLIZATION TECHNIQUES

Sponsored by
Defense Advanced Research Projects Agency
ARPA Order No. 3018

February 1978

The views and conclusions contained in this document are those of the authors and should not be interpreted as necessarily representing the official policies, either expressed or implied, of the Defense Advanced Research Projects Agency or the U. S. Government

CENTER FOR MATERIALS RESEARCH

STANFORD UNIVERSITY • STANFORD, CALIFORNIA

CMR-78-4

FINAL TECHNICAL REPORT

(LONG RANGE MATERIALS RESEARCH) DEVELOPMENT OF ELEVATED TEMPERATURE ELECTROCRYSTALLIZATION TECHNIQUES

Sponsored by

Defense Advanced Research Projects Agency

ARPA Order No. 3018, Amendment No. 4

Program Code Number: 5D10

Contractor: Leland Stanford, Jr. University

Effective Date of Contract: June 1, 1975

Contract Expiration Date: December 31, 1977

Contract Number: N00014-75-C-1171

Principal Investigator: Robert A. Huggins
Phone: (415) 497-4118

Short Title: Long Range Materials Research

February 1978

Center for Materials Research
Stanford University
Stanford, California 94305
(415) 497-4118

SECURITY CLASSIFICATION OF THIS PAGE *(When Date Entered)*

REPORT DOCUMENTATION PAGE

READ INSTRUCTIONS BEFORE COMPLETING FORM

1. REPORT NUMBER: Final Technical

2. GOVT ACCESS

(9) Final rept. 1 Jun 75-31 Dec 77,

(6) 4. TITLE *(and Subtitle)*: (LONG RANGE MATERIALS RESEARCH) Development of Elevated Temperature Electrocrystallization Techniques.

5. TYPE OF REPORT & PERIOD COVERED: Technical (6/1/75-12/31/77)

(14) 6. PERFORMING ORG. REPORT NUMBER: CMR-78-4

(10) 7. AUTHOR(s): Robert A. Huggins, D. Elwell, R. S. Feigelson, R. C. De Mattei

(15) 8. CONTRACT OR GRANT NUMBER(s): N000 14-75-C-1171, ARPA Order-3078

9. PERFORMING ORGANIZATION NAME AND ADDRESS: The Board of Trustees of the Leland Stanford Jr. University, c/o Sponsored Projects Office, Stanford, CA 94305

10. PROGRAM ELEMENT, PROJECT, TASK AREA & WORK UNIT NUMBERS: NR 039-128/12-20-76(471)

11. CONTROLLING OFFICE NAME AND ADDRESS: Director, Metallurgy Program, Office of Naval Research, Department of the Navy, Arlington, VA. 22217

(11) 12. REPORT DATE: Feb [redacted]78

13. NUMBER OF PAGES

14. MONITORING AGENCY NAME & ADDRESS *(if different from Controlling Office)*: Office of Naval Research Resident Representative Stanford University, Room 165 Durand Building Stanford, CA 94305 SCD-C

15. SECURITY CLASS. *(of this report)*: U (12) 53p.

15a. DECLASSIFICATION/DOWNGRADING SCHEDULE

16. DISTRIBUTION STATEMENT *(of this Report)*

Approved for Public Release: Distribution Unlimited.

17. DISTRIBUTION STATEMENT *(of the abstract entered in Block 20, if different from Report)*

18. SUPPLEMENTARY NOTES

19. KEY WORDS *(Continue on reverse side if necessary and identify by block number)*

Molten Salt Electrocrystallization, Growth Stability, Rate-Determining Step, Electrochemical Czochralski Technique, Tungsten Bronzes, Lanthanum Hexaboride Niobium Alloys, Silicon, Gallium Phosphide, Gallium Arsenide, Solid Solutions.

20. ABSTRACT *(Continue on reverse side if necessary and identify by block number)*

The aim of this program was to develop the techniques and understanding necessary for the growh of films or single crystals of a variety of materials by molten salt electrocrystallization.

(over)

(continued)

DD FORM 1 JAN 73 1473 EDITION OF 1 NOV 65 IS OBSOLETE S/N 0102-014-6601

SECURITY CLASSIFICATION OF THIS PAGE *(When Data Entered)*

400 827

The conditions for stable growth of materials by this technique have been explored both theoretically and experimentally. The theoretical studies have shown the importance of a high solute concentration, the potential gradient at the crystal-solution interface and of a material parameter which we have termed the growth rate constant. The current density, which determines the rate of deposition, is also a crucial parameter in many experiments and a value in the range 10-50mA/cm^2 must not be exceeded if stable growth is to occur.

A procedure has been outlined for determining the rate-determining step in electrocrystallization and has been applied to a small number of materials.

A novel experimental technique for the growth of large crystals of uniform cross section, the electrochemical Czochralski technique, was developed.

Crystals of LaB_6 were grown for the first time to a size several mm on edge. PrB_6 films were also deposited.

Attempts to grow $NbGe_3$ as a single phase were not successful although it could be deposited together with other phases.

Silicon epitaxial layers of good morphology were deposited from a fluoride bath. Conditions for the stable growth of epitaxial GaP layers were established, and these two studies were considered of importance in establishing electrochemical epitaxy as a crystal growth technique.

Gallium arsenide was deposited by molten salt electrolysis for the first time.

Attempts to prepare gallium arsenide/phosphide solid solutions yielded a mixture of the two end members.

TABLE OF CONTENTS

A. Introduction

The general aim of this program was to develop the techniques and understanding necessary for the preparation of a variety of materials by electrolysis of molten salt systems at elevated temperatures.

The potential advantages of electrodeposition are numerous. The temperatures required are convenient in comparison with growth from the pure melt, and the deposition is insensitive to minor changes in temperature so that close temperature control is not required. The growth rate is controlled by electrical parameters, which provides the opportunity for precise control and for rapid variation and also allows great flexibility, for example by the use of pulse techniques. In addition, electrical measurements may be used to obtain an understanding of the growth mechanism.

During the course of the program very substantial advances have been made in understanding the theory of molten salt electrodeposition and, as a result of these investigations, it is possible to state with confidence that the statement contained in a 1972 review (1) that "There is little understanding of the factors governing crystal growth by this technique," is no longer valid. In addition a new experimental technique, involving the pulling of crystals of uniform cross section, has been developed and the example of LaB_6 has shown that large crystals of relatively difficult materials can be prepared given a careful investigation. The range of materials which can be crystallized by molten salt electrolysis has been extended, notably by the addition of gallium arsenide, and it has been shown for the first time that uniform epitaxial layers of gallium phosphide can be deposited.

B. Advances in the Theory of Molten Salt Electrocrystallization

The growth of single crystals or epitaxial films requires a knowledge of the conditions under which stable growth may proceed. In the case of electrocrystallization from molten salts, unstable growth is likely to result in the entrapment of solvent inclusions or even in dendritic growth with branching protuberances on the growth interface. In addition, the experimenter wishes to know which of the various processes which contribute to the growth mechanisms is rate-determining, so that the growth conditions may be optimized. In this section the various approaches to these problems which have been made in the program will be summarized, together with the results of experiments which relate directly to these approaches.

1. Electrochemical Analog of Supersaturation Gradient Criterion

The problem of the breakdown of a plane interface which is crystallizing from a fluid phase has been examined by various authors. In the case of growth from the solvent phase the condition for stable growth can be approximated by the constitutional supercooling criterion (2) which relates the maximum rate of stable growth to the temperature gradient in the liquid at the interface. When growth of the solute phase is considered, the similar condition that a protuberance on an otherwise plane surface should encounter a decreasing supersaturation if it is to decay with respect to the surface also relates the maximum rate of stable growth to the temperature-gradient(3). Since the driving force for crystallization is related to the chemical potential, a more general condition for stable growth of a plane crystal surface at $x = 0$ in the x direction is that (4)

$$(d\mu/dx)_{x=o} \lesssim 0 \qquad (1)$$

where μ is the chemical potential of the crystallizing species in the liquid phase.

In the related case where solute is deposited by electrocrystallization from a solution, the solute M is present as M^+ ions (taking the simplest case) in a solvent which may be considered as a fully ionized salt AX.

The electrolytic process may be represented by

$$M^+ + e^- \rightarrow M \qquad (2)$$

and is operated under conditions such that the decomposition potential of the salt AX is not exceeded. Growth proceeds isothermally and in a uniform temperature distribution, so that temperature gradients may be neglected. Crystallization involves the production of an electrically neutral product M from equal numbers of electrons and M^+ ions. The chemical potential which is important is that of the neutral species M which is crystallizing. The stability condition can be written

$$\frac{d\mu_M^+}{dx} = \frac{d\mu_M^+}{dx} + \frac{d\mu e^-}{dx} \lessapprox 0 \qquad (3)$$

where the chemical potential of the neutral M has been written as the sum of terms relating to the electrons and the M^+ ions. If the solution is assumed to be ideal, then $\mu_M^+ = \mu^\circ + RT \ln n$ where μ° is a standard potential and n the fractional concentration of the species in the liquid. The assumption of a zero temperature gradient give

$$\frac{d\mu_M^+}{dx} = \left(\frac{\partial \mu}{\partial n}\right)_T \frac{dn}{dx} = \frac{RT\rho_L}{N_L} \cdot \frac{v(N_S - N_L)}{D\rho_L} \qquad (4)$$

where N_L and N_s are the concentration of M^+ ions in the liquid and solid phase respectively, ρ_L the atomic density of the liquid, D the diffusion coefficient of the ions and v the linear growth rate of the depositing M species. The chemical potential gradient for the electrons is -e dV/dX, with e the electron charge and dV/dX the effective applied potential gradient at the interface. If this is substituted with eq. (4) into eq. (3), the condition for stable growth becomes

$$v \lessapprox \frac{De}{RT} \frac{N_L}{(N_S - N_L)} \left(\frac{dV}{dx}\right)_{eff} \qquad (5)$$

Experimental confirmation of eq. (5) would be difficult because of the inherent problems in evaluating the electron concentration gradient in the neighborhood of the crystal surface.

The stability condition may, however, be envisaged qualitatively from fig. 1. This shows that a sufficiently large voltage gradient must be applied to prevent the occurrence of a supersaturated region ahead of the interface.

As in conventional crystallization, stability is enhanced by increasing the solute concentration N_L. A high diffusion coefficient (which is directly proportional to the ionic mobility) is also desirable. The temperature dependence of the maximum stable growth rate is governed primarily by the term D/T and is, therefore, more difficult to predict, but stability is normally enhanced slightly by increase of temperature.

The most significant feature of eq. (5) for the growth of high quality crystals by electrodeposition is the requirement of a high electric potential gradient at the crystallizing surface. Stirring the solution is expected to increase the local electric potential gradient by reducing the thickness of the boundary layer. If growth occurs at constant cell voltage (or overpotential), stirring is likely to increase the growth rate v, perhaps without affecting interface stability. If the current density is maintained constant, however, dV/dx may be increased independently of v.

Higher stable growth rates than those predicted by eq. (5) will be possible if additional stabilization results from the capillary effect. As in the case of crystallization using a thermal driving force, stabilization is expected to be particularly enhanced if growth occurs on facetted crystals by the propagation of layers across the surface. Facetting is observed in the growth of crystals of, for example, boride and tungsten bronze crystals grown by electrodeposition but is not so important in the deposition of metallic coatings. Particularly in the latter case, a strong departure from stable growth conditions can lead to powder formation. The degree of supersaturation is sufficient in this case to cause nucleation of separate powder particles ahead of the interface. These may be entrapped in the advancing solid, with a high concentration of included solvent, or may be carried away by motion of the bulk fluid outside the boundary layer.

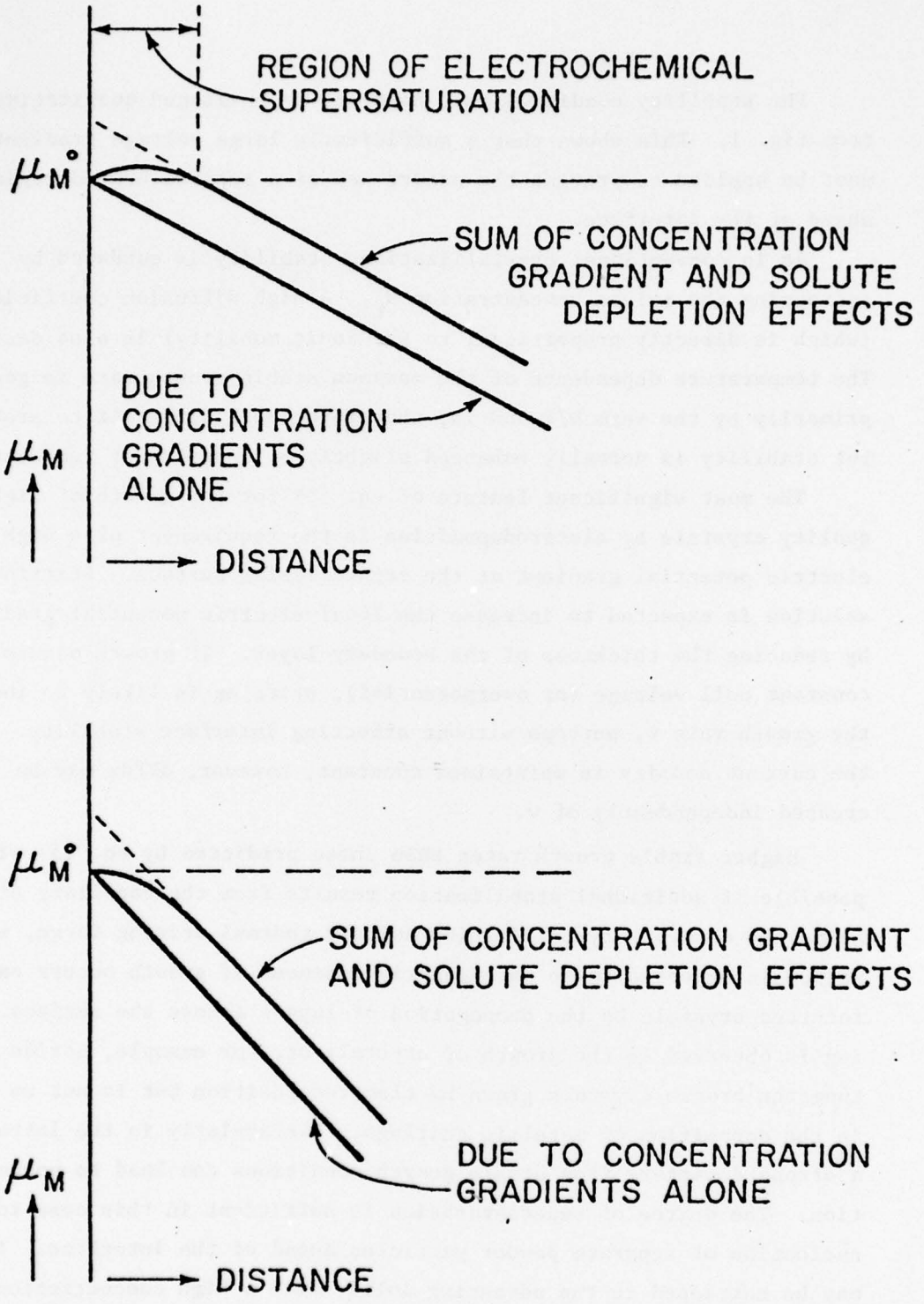

Figure 1. Chemical potential profiles ahead of crystal surface, for unstable (upper) and stable (lower) growth by electrocrystallization.

2. The Critical Growth Rate Constant

As stressed in the preceding section, crystallization in an optimized system will proceed at a value just below the maximum value for stable growth. In attempting to apply this condition in practice to various systems, the concept was found useful of the growth rate constant K, defined by the equation

$$v = K\varepsilon i \tag{6}$$

where i is the current density and ε the efficiency of deposition. According to Faraday's law, the volume of material deposited electrochemically is

$$V = M\varepsilon q/\rho zF \tag{7}$$

where M is the molecular weight of the depositing material, ρ its density, z the number of electrons transferred per unit of material deposited, F Faraday's constant, ε the efficiency of deposition and q the total charge transferred in coulombs. Thus, it may be simply shown that

$$K = \frac{M}{\rho nF} \tag{8}$$

When multiplied by 3600 sec/hr, K has the units cm^3/amp-hr. The value of K is fixed by the material deposited and the electrochemical process involved.

It should be noted that in eq. 6 the value of ε may not be constant under all experimental conditions. In particular, ε may be a function of temperature, as it is with the sodium tungsten bronzes (5,6). In the discussion which follows, except where noted, the value of ε is assumed constant and equal to 1. This is a limiting case and deviations from this value only produce a less desirable situation. The value of K for sodium tungsten bronze is around 2·0 cm^3/amp.hr. depending on the composition, and it was found possible to pull crystals of constant diameter at rates of up to 3 mm/hr. The deposition of metals by the electrochemical Czochralski technique (7) was studied in order to investigate the range of materials that could be grown by this technique. In addition, metals have isotropic growth kinetics and it was predicted that crystal

morphology and diameter control would differ significantly from the tungsten bronzes.

Initially niobium was chosen as a model system for ECT growth since it is representative of metals with close to isotropic growth behavior. Niobium can be deposited electrochemically at 700°C from a melt consisting of an equimolar eutectic of lithium fluoride (LiF) and potassium fluoride (KF) as the solvent for 6 mole % potassium niobium fluoride (K_2NbF_7). Growth of niobium by ECT was, however, very difficult. Unfortunately niobium has a growth rate constant K of 0.1011 cm/amp-hr. which requires a very large current density of 989 mA/cm^2 to pull a crystal at 1 mm/hr. At this current density a stable interface cannot be maintained and a powdery deposit would probably result. Even at the very slow growth rate of 0.1 mm/hr used in these experiments, the current density is in the regime that would cause dendritic growth. To promote stable growth at this growth rate, a previously developed electropolishing technique was applied during ECT growth (Fig. 2). The principle of this technique is to deposit material during the cathodic half cycle at a rather high rate which produces not only a coherent layer but also dendrite precursors. During the anodic or polishing half cycle, these precursors are selectively dissolved in preference to the coherent layer. One of the critical parameters is the ratio between growth and dissolution, Q. As this parameter approaches 1, the quality of the final layer will improve but the effective growth rate will approach zero. Based on previous work (7) the value of Q was set at 2.

Static experiments were performed on single crystal niobium plates. An average current density of 50 mA/cm^2 at 740 to 750°C was used and oriented single crystal layers were produced. Based on these results, it was decided to use a cathodic period of 25 seconds followed by an anodic period of 10 seconds with cathodic to anodic current ratio of 1 to 1.25, but to vary the actual magnitude of the currents to produce the best results. The seed size was fixed at 3.5 mm x 3.5 mm. After some initial variation, 0.1 mm/hr and 18 rpm were selected as the pull and rotation rates for these experiments. The cathodic current was varied from 15 to 300 mA while the anodic current was varied rrom 18.75 to 375 mA. This produced average currents which ranged from 5.4 mA to

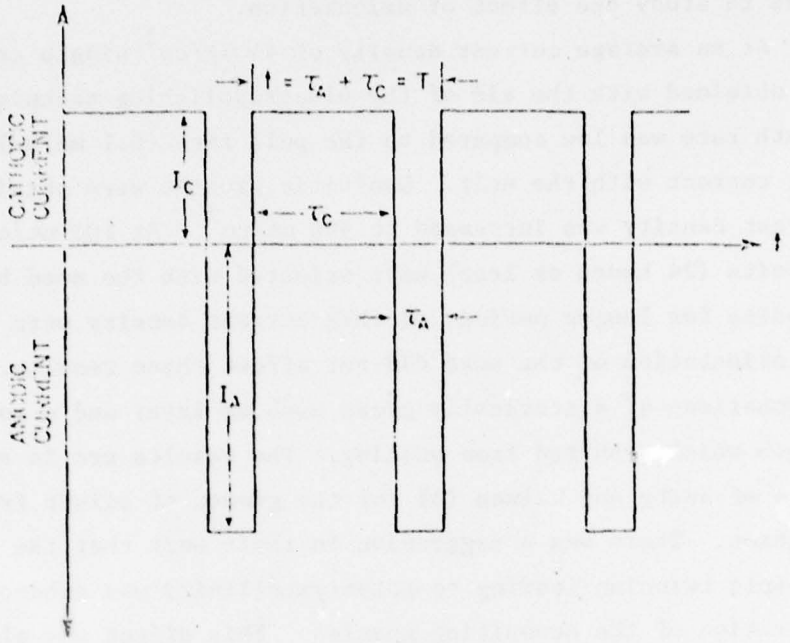

$$Q = \frac{\tau_c I_c}{\tau_a I_a} = 2$$

$$I_{avg} = \frac{\tau_c I_c - \tau_a I_a}{\tau_c + \tau_a} = 5.3 - 150 \text{ ma}$$

$$i_{avg} = 43.7 - 1224 \text{ ma/cm}^2$$

Figure 2. Alternating square wave used for niobium electrodeposition.

107 mA (44 to 900 mA/cm^2). The majority of depositions were made on (110) oriented seeds with two depositions each on (100) and (111) oriented seeds to study the effect of orientation.

At an average current density of 44 mA/cm^2 single crystal niobium was obtained with the aid of the electropolishing technique, but the growth rate was low compared to the pull rate (0.1 mm/hr) and the crystal lost contact with the melt. Dendritic growths were obtained when the current density was increased to 900 mA/cm^2. At 100 mA/cm^2, short time deposits (24 hours or less) were oriented with the seed but twinned. Deposits for longer periods at this current density were polycrystalline. The orientation of the seed did not affect these results. Figure 3 is a comparison of a statically grown niobium layer and a polycrystalline growth which resulted from pulling. The results are in agreement with those of Setty and Wilman (8) for the growth of silver from aqueous solution. There was a suggestion in their work that the tendency to multiple twinning leading to polycrystallinity was enhanced by a low concentration of the depositing species. This effect was also predicted by the study of morphological stability described in the previous section.

The niobium melt used in these experiments contained only 0.6 atomic % niobium. In order to have a system with higher metal ion concentration, the deposition of iron (K = 0.125 cm^3/amp-hr) from a ferrous chloride (55 mole % $FeCl_2$) - potassium chloride (KCl) eutectic was investigated. All of the growths in the study of the iron system were done without pulling or rotation. The initial depositions were done without electropolishing at 410 to 420°C. The current density varied from 20 to 50 mA/cm^2. The deposits were all dendritic. Electropolishing using a cathodic current of 112 mA for 5 seconds followed by an anodic current of 140 mA for 2 seconds (40 mA/cm^2 average current density) was tried. A dendritic deposit again resulted. To reduce the possibility of viscosity-induced diffusion effects, the temperature was raised to 610°C and the experiment was repeated with the same results. Since solubility alone did not appear to permit stable growth at moderate current densities, the limiting property appeared to be the low value of the growth rate constant of both niobium and iron.

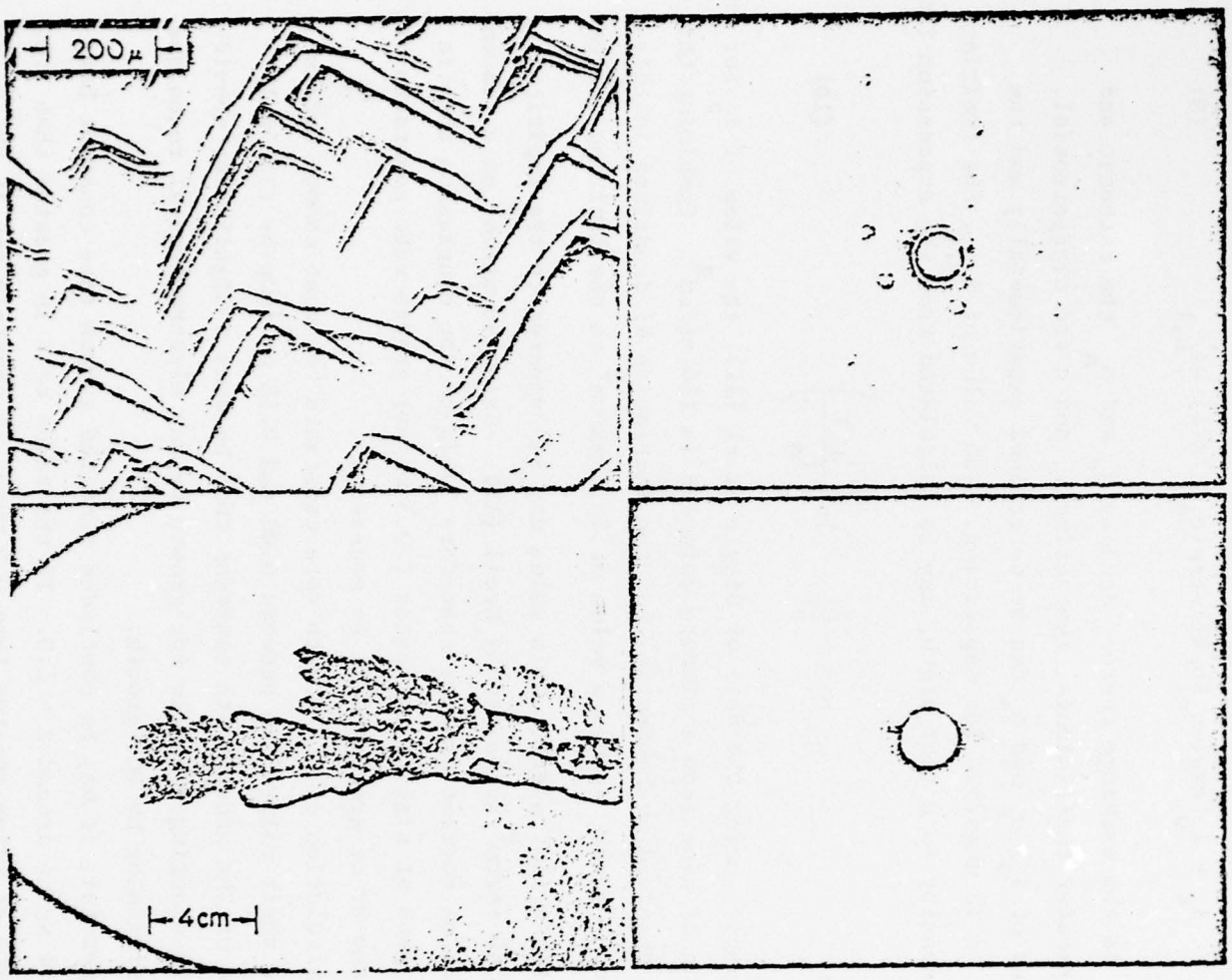

Figure 3. Single crystal niobium layer (upper) and polycrystalline growth resulting from pulling (lower). Corresponding Laue photographs to the right.

Throughout all of these studies, there is the problem of limiting current densities which cannot be exceeded. In the case of dendritic growth the critical current density (i_c) may be calculated (9) from the expression

$$i_c = i_0[\exp(-\alpha_c F\eta/RT)-\exp(\alpha_a F\eta/RT)] \geq i_{L,1} \qquad (9)$$

where i_o is the exchange current density, α_c and α_a the cathodic and anodic transfer coefficients, respectively, and η the overpotential. The values of i_o, α_c and α_a can be determined experimentally and the value of η is negative for deposition. The value of $i_{L,1}$, the limiting current density to a flat plate, may be calculated from the expression (10)

$$\eta = \frac{RT}{zF} \ln\left(\frac{i_{L,1}}{i_0}\right) \qquad (10)$$

As an example, using the data of Diggle et al (11), the value of i_o for the deposition of zinc from a zincate solution is 250 mA/cm^2. Combining this with the observed overpotential for the initiation of dendrites in this system (η = -60mv), gives a value of 43.5 mA/cm^2 as the limiting current density for a flat plate. This value may be compared to the empirical value of 40 mA/cm^2 suggested by Kroll (12). Using 40 mA/cm^2 as a reasonable limit on current density therefore leads to the conclusion that in order to grow at significant rates (>0.5 mm/hr) growth rate constants of 1.0 cm^3/amp-hr or greater will be necessary.

A calculation of the growth rate constants for most common metals show that their values lie between 0.08 and 0.38 cm^3/amp-hr (Table I). The value of the growth rate constant thus becomes a significant consideration in choosing a system for growth by any electrochemical technique and in particular by ECT growth.

In general, it may be concluded that the growth rate constant has a critical value around K = 1.0. If the value of K is greater than 1.0, then growth at rates greater than 0.5 mm/hr is possible and if the value of K is less than 1.0, then either a slow growth rate must be tolerated or the growth rate must be optimized by varying process parameters such as concentration, electropolishing parameters and stirring.

Table I. GROWTH RATE CONSTANTS (K) OF SOME COMMON METALS

Metal	K(cm^3/amp-hr)
Aluminum	0.124
Bismuth	0.265
Boron	0.057
Chromium (n=2)	0.135
(n=3)	0.090
Cobalt (n=2)	0.124
(n=3)	0.082
Copper (n=1)	0.266
(n=2)	0.133
Gallium	0.147
Germanium (n=2)	0.253
(n=4)	0.127
Gold (n=1)	0.432
(n=3)	0.144
Iron (n=2)	0.133
(n=3)	0.088
Lead (n=2)	0.341
(n=4)	0.170
Magnesium	0.261
Manganese (n=2)	0.142
(n=3)	0.095
Molybdenum (n=2)	0.175
(n=3)	0.117
(n=4)	0.088
Nickel	0.123

Metal	K(cm^3amp-hr)
Niobium (n=3)	0.135
(n=4)	0.101
(n=5)	0.081
Platinum (n=2)	0.170
(n=4)	0.085
Silicon	0.112
Silver	0.383
Tantalum (n=4)	0.102
(n=5)	0.081
Tin (n=2)	0.304
(n=4)	0.152
Titanium (n=2)	0.199
(n=3)	0.132
(n=4)	0.099
Tungsten (n=2)	0.177
(n=4)	0.089
(n=5)	0.071
(n=6)	0.059
Zinc	0.171

By way of example, consider the two commercially prominent electrochemical processes: The Hall process for aluminum production and the electrorefining of copper. In the case of aluminum, current densities in excess of 1000 mA/cm^2 are routinely employed. In order to avoid problems with morphology, the process temperature is raised so that the aluminum is molten. In the case of copper, the current density is low (12 to 15 mA/cm^2) and high production rates are achieved through the use of large cathode areas. The production of aluminum represents a case of variation of process parameters, while copper refining is an example of accepting a slow growth rate.

3. The Rate-Determining Step

Crystal growers faced with the problem of designing an experiment to produce crystals of a specified material are particularly interested in the rate-determining step, which is the slowest step in the sequence leading to crystallization. The convenience of electrical measurements may permit the rate-determining step to be identified more readily in electrocrystallization than in solution growth using a thermal driving force. This topic has been discussed in the annual Technical Report of January 1977 (CMR-77-1) where attention was drawn to the value of measurements of current versus overpotential during growth, including data as a function of the crystal rotation rate in the Czochralski or "top-seeded" geometry.

The steady-state current I during electrocrystallization may, in general, be expressed in the form

$$I = \eta(R_{vd} + R_{ct} + R_{ik})^{-1} \qquad (11)$$

Here R_{vd}, R_{ct} and R_{ik} are resistances associated respectively with the volume diffusion, charge transfer and interface kinetic processes, the latter including desolvation, surface diffusion and integration at kink sites. The effective values of these resistances are difficult to obtain from first principles, but the origin of the rate-determining component may be identifiable from the $I(\eta)$ data. Here the analogy is useful between electrocrystallization and conventional solution growth. The flow of crystallizing material is clearly related to the flow of

current, and the linear growth rate v of a crystal of surface area A depends upon the current I according to the relation

$$v = \frac{\varepsilon I \Omega}{zFA} \tag{12}$$

where Ω is the molar volume.

The overpotential η represents the driving force for crystallization and it is convenient to associate η directly with the relative supersaturation σ. An ohmic resistance is therefore associated in this analogy with a linear relation between v and σ.

The volume diffusion component R_{vd} is expected to be ohmic since eq. (2) may be rewritten as

$$i = \frac{DzF\sigma n_e}{\delta} \tag{13}$$

with n_e the equilibrium concentration of solute δ and with $v \propto i = I/A$ according to eq. (12).

In general, the charge-transfer component R_{ct} will be non-ohmic as the current is given by the difference of two exponential terms, as in eq. (9). The term R_{ik} of eq. (11) will also be non-ohmic in the general case since, for growth on a surface intersected by screw dislocations, the relation between v and σ is (13)

$$v = \frac{C\sigma^2}{\sigma_1} \tanh \frac{\sigma_1}{\sigma} \tag{14a}$$

where C and σ_1 are constants of the material and conditions. At low values of σ ($\sigma << \sigma_1$), eq.(14a) approximates to a quadratic variation

$$v = C\sigma^2/\sigma_1 \tag{14b}$$

The model outlined above was tested by application to sodium tungsten bronzes and to lanthanum hexaboride, LaB_6. Figure 4 shows I versus η data for bronzes of composition Na_xWO_3 with x = 0.61 and x = 0.73. The solid lines were fitted by assuming that $R_{vd} >> R_{ct} + R_{ik}$ during dissolution but that $R_{vd} \sim R_{ik} >> R_{ct}$ during crystallization. The dissolution data indicate an ohmic resistance while the crystallization data exhibit a strong departure from ohmic behaviour. An acceptable fit to the crystalli-

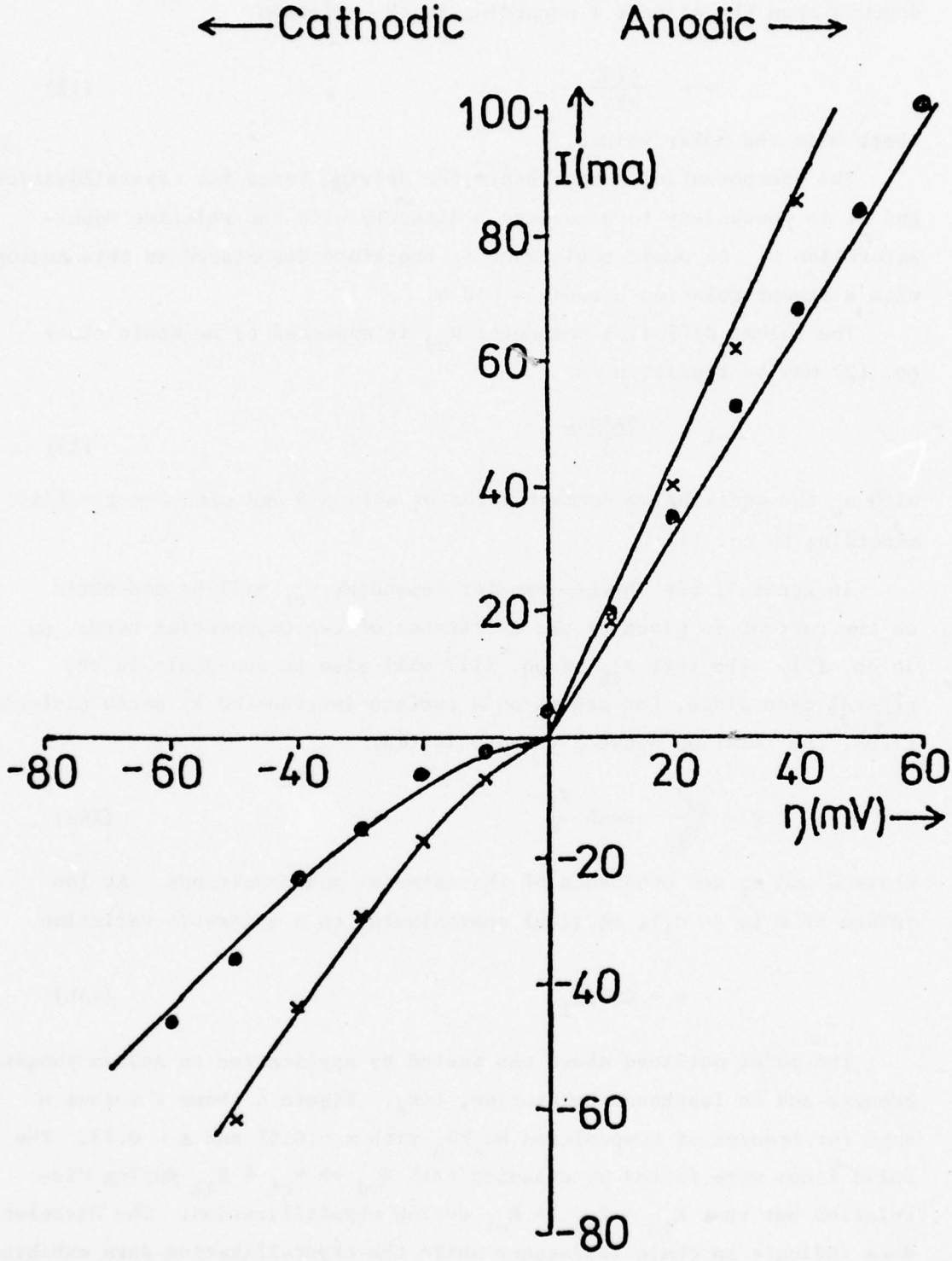

Figure 4. Current versus overpotential for tungsten bronzes: (o) $Na_{.61}WO_3$ (x) $Na_{0.73}WO_3$. Cathodic curves are calculated using $R = 0{\cdot}612 + 0{\cdot}164I^{-\frac{1}{3}}$ and $R = 0{\cdot}458 + 0{\cdot}093 1I^{-\frac{1}{3}}$ ohms respectively.

cation data was obtained by assuming the analog of eq. (14b) for R_{ik}, namely that $I \propto \eta_{ik}^{2}$ so that

$$R_{ik} \propto I^{-\frac{1}{2}} \qquad (15)$$

where η_{ik} is the overpotential associated with the interface kinetic process. In fitting the cathodic data, the same volume diffusion component R_{vd} as in dissolution was added to a term R_{ik} calculated according to eq. (15) . Confirmation of the postulate that the ohmic component is due to volume diffusion was obtained by measurements of the current during crystallization on a seed rotated about the <111> axis. Although the rotation introduces additional scatter in the data, Fig. 5 is in agreement with the assumption that the resistance has a component independent of the rotation rate ω and one which varies as $\omega^{-\frac{1}{2}}$. The relation $R_{vd} \propto \omega^{-\frac{1}{2}}$ is expected from the well-known variation with ω of the thickness δ of the boundary layer. In electrochemistry, this variation is normally associated with the theory of Levich (14) which is mainly applied to measurements using a rotating disc electrode in aqueous solutions.

In the case of LaB_6, the dissolution behaviour is strongly non-ohmic and the assumption made in this case was that $R_{ct} >> R_{vd} + R_{ik}$. Figure 6 shows the experimental data, with the dashed line plotted according to

$$I = 7.36 \sinh(3.5\ \eta F/RT) \quad (mA) \qquad (16)$$

The difference between the dashed curve and the cathodic data is assumed to be due to the component R_{ik}, which becomes comparable with R_{ct} during crystallization. A reasonable fit to the crystallization data is obtained by adding to the R_{ct} term defined by eq. (16) a term R_{ik} which varies as $I^{-\frac{1}{2}}$ as for the tungsten bronzes.

The relatively complex charge transfer process indicated by eq. (16) is not unexpected since the formation reaction is itself complex. The value of 3.5 in the sinh term of eq. (16) is consistent with a rate-determining step in the charge-transfer reaction which is repeated 3 times in the formation of an LaB_6 molecule.

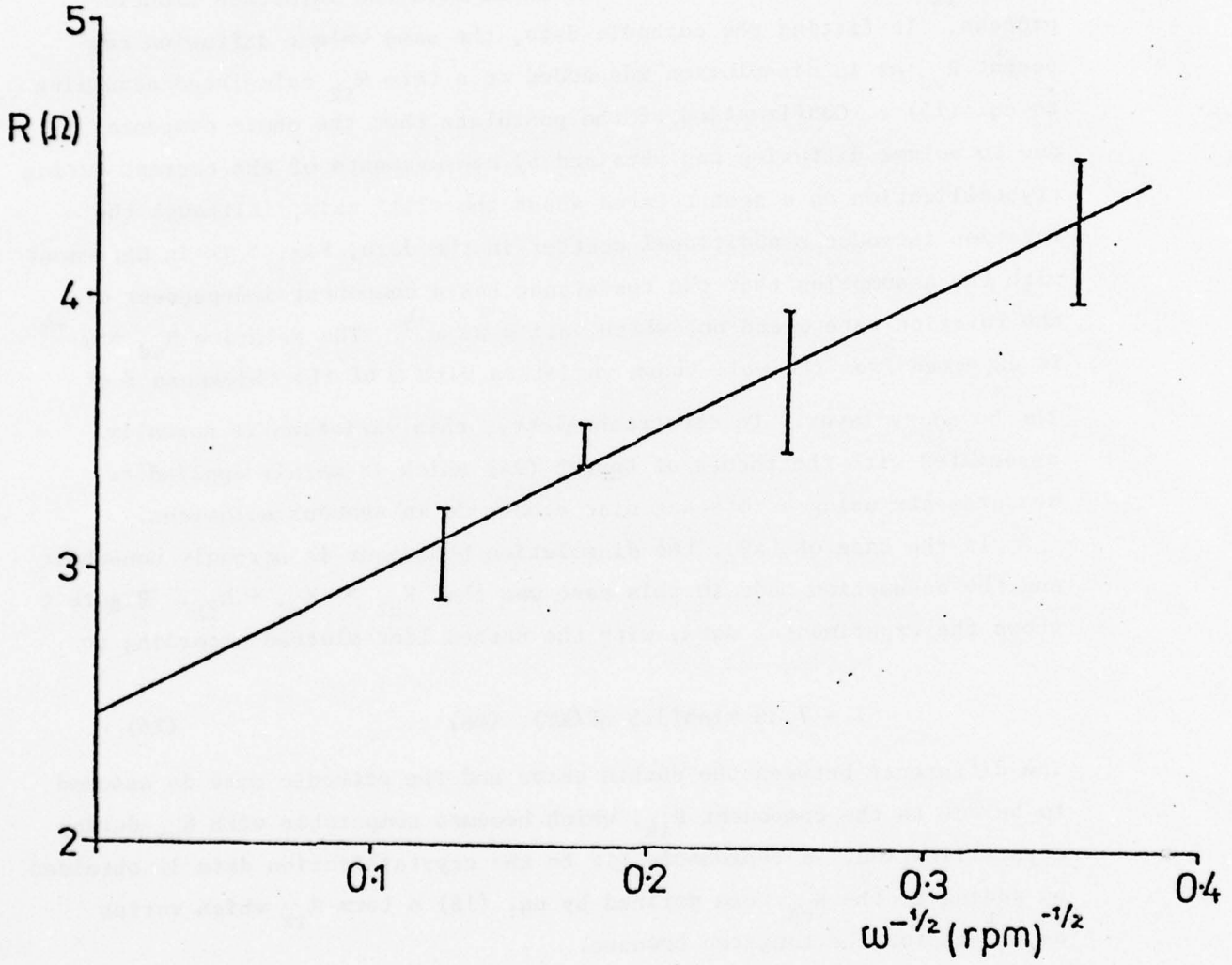

Figure 5. Variation of resistance for tungsten bronze electrodeposition with $\omega^{\frac{1}{2}}$ (ω the crystal rotation rate).

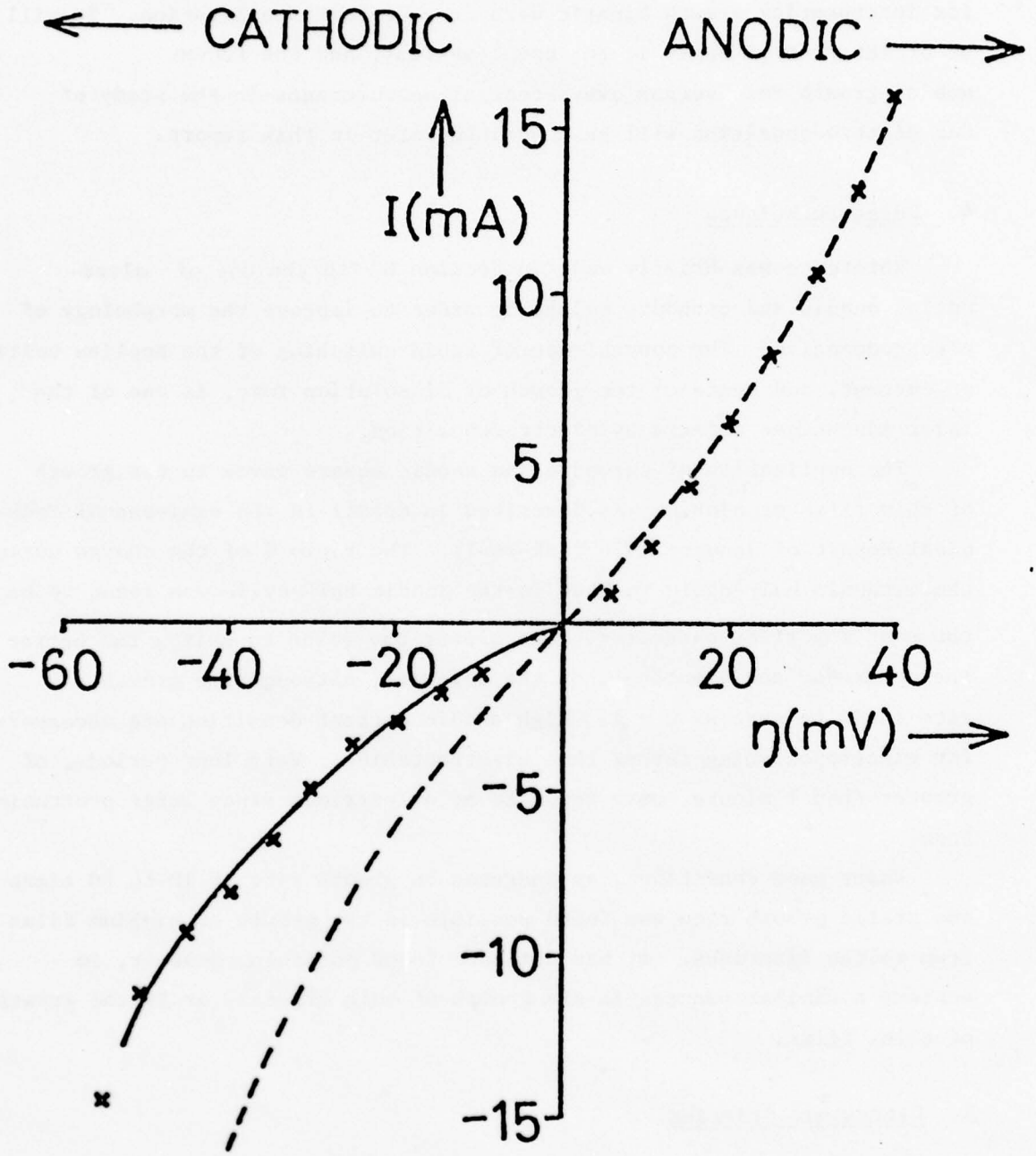

Figure 6. Current versus overpotential for LaB_6.

The approach outlined above provides a simple but powerful tool for interpreting growth kinetic data in electrocrystallization. It will be of interest to apply it to novel systems, and the recent use of growth rate versus overpotential measurements in the study of GaP electrodeposition will be described later in this report.

4. Pulse Techniques

Reference was briefly made in Section B2 to the use of alternating anodic and cathodic pulses in order to improve the morphology of electrodeposits. The convenience of rapid switching of the applied voltage or current, and hence of the growth or dissolution rate, is one of the major advantages offered by electrodeposition.

The application of cathodic and anodic square waves to the growth of thin films of niobium was described in detail in the semi-annual Technical Report of January 1976 (CMR-76-1). The ratio Q of the charge during the cathodic half-cycle to that in the anodic half-cycle was found to be the most important parameter. The closer the value to unity, the better the coherency and smoothness of the deposits, although the growth rate tends to zero as $Q \rightarrow 1$. High anodic current densities are necessary for electropolishing rather than electroetching. Very long periods, of greater than 1 minute, were found to be deleterious since large protrusions form.

Under good conditions, an increase in growth rate of 10 to 50 times the static growth rate was found possible in the growth of niobium films from molten fluorides. It has not been found possible, however, to achieve a similar success in the growth of bulk crystals or in the growth of alloy films.

5. Ultrasonic Stirring

In addition to the use of a rotating cathode and of ac potentials, the effect was studied of ultrasound on the morphology of the deposit. The use of ultrasonics as a means of stirring a solution and improving crystal growth was proposed by Kaputsin (15), who investigated the effects

of ultrasound on the kinetics of crystallization from aqueous solution and on crystal habit. The results of our investigation are summarized in the first annual Technical Report (CMR-74-6). The major findings were that the overpotential exhibited a minimum at a power level of about 20 watts at $24KH_z$, and that the cathode efficiency decreased rapidly at power levels above this value. The ultrasonic energy was, in all cases, more effective in decreasing overpotential than the theoretically predicted value, indicating that there may be a decrease in the boundary layer thickness. Significant improvements in the morphology of zinc deposits from an aqueous zincate solution were not obtained.

C. Advances in Experimental Technique

The majority of the experiments described in this report were performed on simple and inexpensive apparatus. In fact, the absence of a requirement for expensive equipment is seen as one of the advantages of molten salt electrocrystallization.

The only major advance in experimental technique during the course of this program was the development of the electrochemical Czochralski technique (ECT) which was described in detail in the Semi-annual Technical Report of June 1975 (CMR-75-13).

Czochralski developed the technique of pulling crystals from the melt and his name is now associated with a method of crystal growth which has very wide applicability. Recent developments of this method have been particularly concerned with the automatic production of crystals of uniform cross-sectional area. In electrocrystallization it was considered possible to pull crystals of constant diameter by a suitable choice of operating conditions, with simple control of electrical parameters rather than by use of relatively complicated weighing sensors or infrared detectors. This goal was realized in the case of sodium tungsten bronze crystals, with the apparatus shown diagrammatically in Fig. 7.

The use of a constant current supply was found to give effective control of the crystal diameter for crystals grown in a [111] direction. The growing crystal surface is made up of (100) facets, since the tungsten bronzes exhibit a very strong tendency towards facet formation. The form of the crystals is very sensitive to the orientation of the seed crystal, and very slight misorientations can lead to deviations of the crystal from axial symmetry.

Stable growth of tungsten bronze crystal by the ECT was found to be possible at rates of up to 3mm/hr. This is extremely rapid for any process of crystal growth from solution and is comparable with rates of growth from the melt. According to the stability criteria discussed in Section B, it is unlikely that such rapid rates will be possible for systems in which the solute concentration is low, or where the growth rate constant K lies below unity.

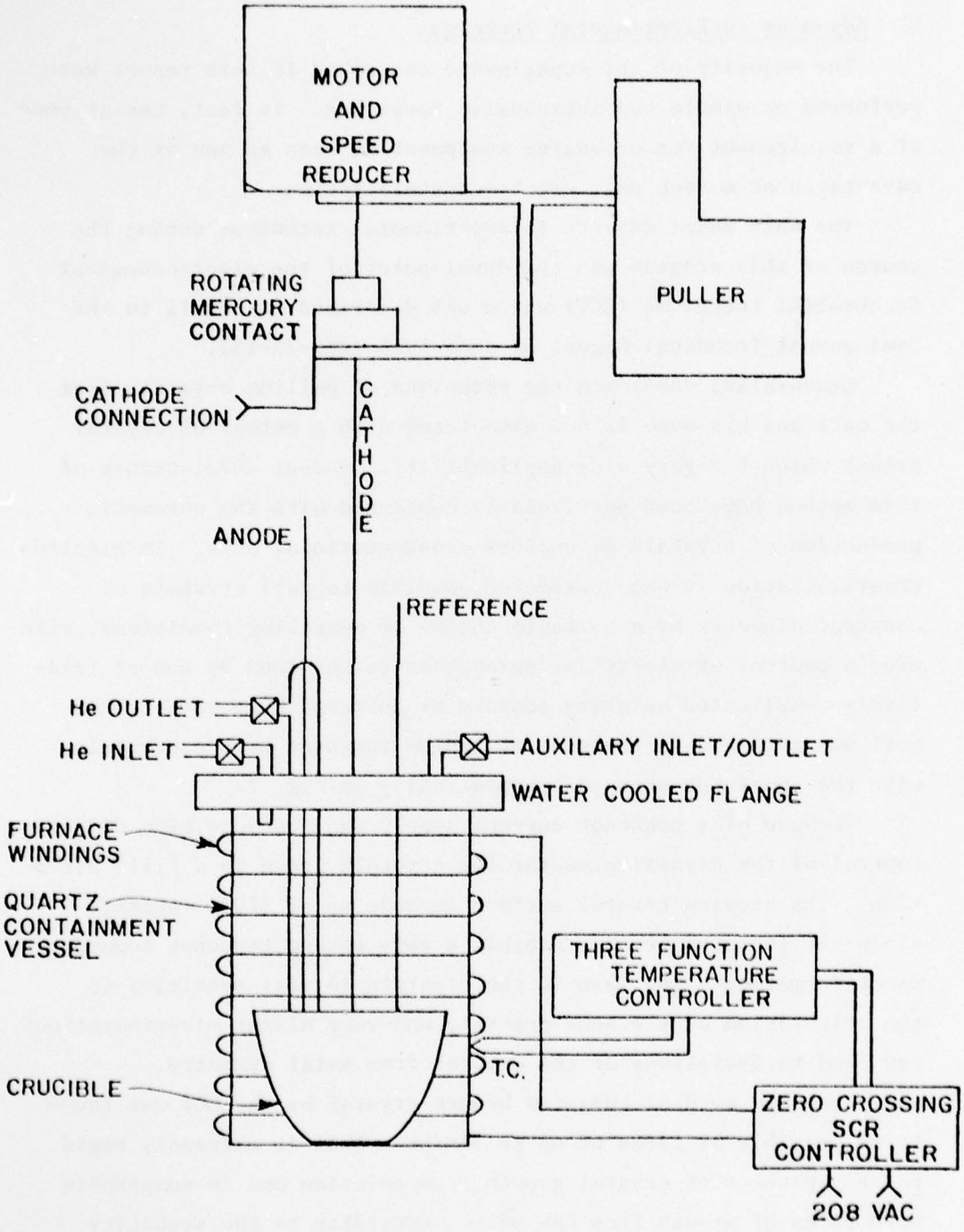

Figure 7. Apparatus used for the Electrochemical Czochralski Technique (diagrammatic).

In spite of these limitations, the ECT represents a significant development in molten salt electrocrystallization and may eventually be applied, for example, to the growth of indium phosphide.

D. Studies of Particular Materials

1. Lanthanum Hexaboride LaB_6

The growth of large crystals of LaB_6 was one of the major achievements of this program and required a detailed and intensive study of the molten salt system, nucleation, stability of growth and the effects of electrical and other system parameters on the growth conditions. This study is described in the Technical Reports for 1974 and 1975 (CMR-74-2; 74-6; 75-13 and 76-1). Prior to this study, the synthesis of LaB_6 had been reported by molten salt electrolysis but only tiny crystals of less than 1 mm on edge had been produced.

Electrolysis of a bath containing La_2O_3, B_2O_3, Li_2O and LiF produced initially crystallites of about 10 μm in size on a gold wire used as cathode. Grain selection proceeded slowly during growth as some of the smaller crystallites were overgrown and the larger ones continued to grow. After a period of 100 h a deposit would contain clusters of crystallites 1 mm on a side. These would continue to grow, and a cluster would contain 4 mm crystallites after 300 h. The ultimate crystallite size is, therefore, strongly time dependent, and larger crystals need very long growth cycles. Secondary nucleation, which severely limited crystal size, was found to occur if there were significant perturbations in the operating conditions (current, voltage, temperature) of the cell.

During growth at constant potential, the cell current rose continuously. Deposition on the cathode increased the cathode surface area, lowering the resistance of the cell and producing a corresponding rise in current.

The morphological characteristics of individual LaB_6 crystallites were found to vary with current density. The individual crystals in the deposit grow as layers formed at pyramidal sites on the crystal face which spread outward in all directions from their sources (dislocations intersecting the surface). At low to moderate current densities (<25 mA/cm^2) these active centers are located at the interior of the (100) crystal faces and the layers spread outward toward the

edges of the crystallites. As the current density is increased (30-50 mA/cm^2), the active centers become located at the corners and edges of the crystallite, the edges and corners closest to the incoming nutrient. The growing layers spread toward the interior of the (100) crystal face. At high current densities, edge and corner growth is accentuated and hopper growth is prevalent. At extremely high current densities (>100 mA/cm^2) dendrites grow from the corners along the [111] direction. The critical current density for growth of crystals with a stable cubic morphology appears to lie in the region of 30 mA/cm^2. The optimum current density for growth of cubic material was in the region from 15 to 25 mA/cm^2.

The first successful seeded growth was carried out on a rectangular slice of LaB_6 2 x 3 mm in cross section immersed to a depth of 2.5 mm in the melt. After a period of 87 h the seed had well-developed facets and measured ~4 x 5 x 3 mm, an increase in size of ~300%. The same seed was re-introduced into the bath, and totally immersed below melt level. After an additional deposition period of 113 h (current density 18 mA/cm^2) the crystal measured 5 x 6 x 6 mm. By estimating the surface area of the seed the cell voltage could be adjusted so that the initial cathodic current density was ~20 mA/cm^2. Small periodic admustments in cell potential were then made to control the slope of the current versus time curve. A large well-developed crystal of LaB_6 6 x 6 x 5 mm is shown in Fig. 8.

The significance of the first synthesis of fairly large crystals does not lie in the suitability of these crystals for electron emitter or other applications, since long crystals of uniform diameter can now be grown by Hitachi using a molten zone technique. What has been demonstrated by this study is that it is possible to use molten salt electrodeposition for crystal growth of difficult refractory materials, rather than merely as a tool for synthesis.

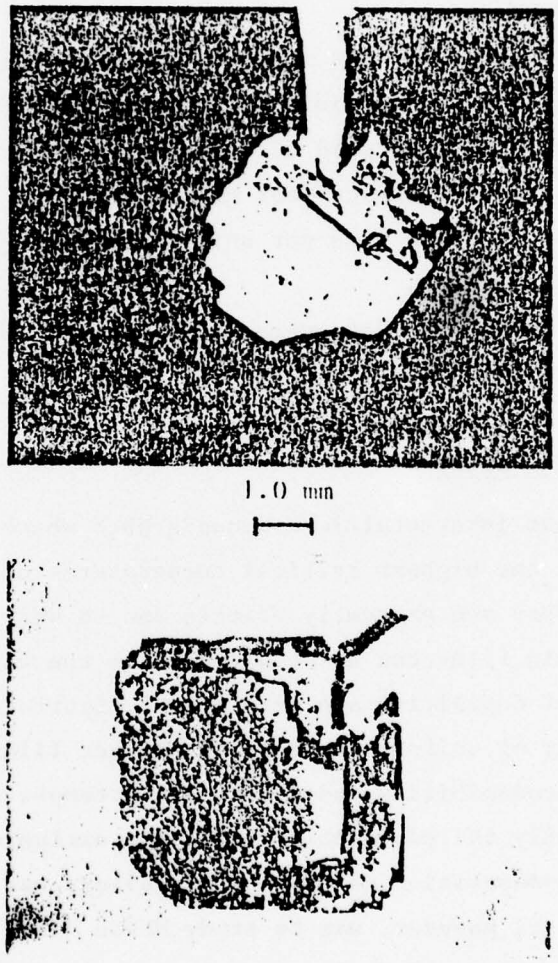

Figure 8. Crystal of LaB_6 6 x 6 x 5 mm in size. The upper photograph shows the same crystal at an earlier stage of growth.

2. Other Borides

Following the success with LaB_6, attempts were made to grow praesodymium hexaboride PrB_6 and scandium diboride ScB_6. These experiments are described in the semi-annual Technical Report of January 1976 (CMR-76-1).

PrB_6 was required in the form of thin layers for Mössbauer studies. Rapid success was initially achieved in the deposition of 1 mm crystallites on a gold wire cathode when Pr_6O_{11} replaced La_2O_3 in the bath used for crystal growth of LaB_6. Subsequently PrB_6 films of controlled mass per unit area were deposited on Ni and graphite substrates.

Attempts to deposit ScB_2 were not successful since deposits were invariably multiphase.

3. Niobium Alloys

The niobium intermetallic compounds Nb_3X where X is Al, Sn, Ge and Si exhibit the highest critical temperatures of all the known superconductors. They are extremely brittle and so very difficult to fabricate. Thin films can be deposited from the vapor phase but the kinetics of deposition are very slow. Electrodeposition offers the possibility of uniform coatings of thicker films, and in principle of greater reproducibility and quality. Attempts to codeposit Nb and Al invariably failed, niobium being the exclusive deposit in all cases. Co-deposition of niobium-tin alloys was demonstrated. The major thrust, however, was to study Nb-Ge alloy deposition and to attempt the synthesis of Nb_3Ge.

Nb_3Ge has a superconducting transition temperature of 23°K which is the highest known value. The technical problems involved in production of wires have prevented the widespread application of this material, in spite of the obvious advantages associated with superconductivity at liquid hydrogen temperatures.

Electrodeposition of Nb and Ge was performed using a solution of K_2NbF_7 with K_2GeF_6 in KF-LiF eutectic. Best results were obtained with a Mo working electrode and a Ge sheet used as counter-electrode.

Nb-Ge alloys were deposited at potentials of -60mV and Nb alone at -300 mV, these potentials being measured with respect to a Mo/Nb(IV), Nb(V) reference electrode. When relatively rich germanium solutions were used, the first cathodic wave showed more than one step, and it was found possible to deposit Nb_3Ge_2, Nb_5Ge_3 or Nb_5Ge_3/Nb_3Ge by electrolysis at constant potential.

Cyclic voltametry was used to establish conditions for the deposition of various Nb-Ge phases and mixtures. These are listed in Table 2. $NbGe_2$ could be deposited readily with relatively large grain size (~20 μm). Single phase Nb_3Ge_2 and Nb_5Ge_2 could also be produced at relatively low potentials, by varying the concentration of germanium in the solution.

The required compound Nb_3Ge, could be deposited only as the minor constituent of a two-phase mixture, together with Nb_5Ge_3 or Nb metal respectively. In the first case, the Nb_3Ge appeared under similar conditions to those used for Nb_5Ge but at the higher temperature of ~815°C.

The deposits were characterized by x-ray diffraction and found to have a lattice parameter of 5·14-5·17 Å, for bulk material. The differences may be due to defects in the electrodeposited samples or to the lower temperatures used in comparison with the bulk material.

In all a total of 29 experiments were performed with 5 m/o K_2NbF_7 and 8 experiments with 80 m/o K_2NbF_7 in specific attempts to deposit single phase Nb_3Ge. These attempts are summarized in Table 3. The first two groups led to stable growth of Nb-Ge alloys, while the third produced Nb alone. Groups 4-6 utilized a large cathodic polarization in an attempt to increase the Nb-Ge ratio in the deposit. In each case, however, unstable growth of dendrites or powders was observed on top of a thin adherent layer. The seventh group includes experiments utilizing the alternating square wave pulse and potential sweep techniques which were performed in attempts to improve the morphology of the deposit, while still utilizing the large cathodic polarization. The latter experiments yielded inconclusive results, with problems associated with the separate stripping potentials

Table 2. Nb-Ge Compound Deposition

Phase(s)	Bath Composition (mol.%)	Temperature (°C)	Electrical[a] Signal	Alloy[b],[c] Composition (mol.%)	X-ray Diffraction Analysis	T_c (°K)	Remarks
$NbGe_2$	Nb 5.000 Ge 0.161	707 ± 2	Constant η = -18 mV	Nb 34.0 - 34.5 Ge 66.0 - 65.5	$NbGe_2$	----	Individual crystallites
$NbGe_2/Nb_3Ge_2$	Nb 5.000 Ge 0.053	703 ± 2	Constant η = -30 mV	Nb 57.8 - 63.5 Ge 42.2 - 36.5 Nb 36.7 Ge 63.3	$NbGe_2$ Nb_3Ge_2	----	Separate Microprobe analysis of the two phase regions
Nb_3Ge_2	Nb 5.000 Ge 0.050	753 ± 2	Constant η = -35 mV	Nb 60.8 - 61.2 Ge 39.2 - 38.8	Nb_3Ge_2	----	
Nb_3Ge_2/Nb_5Ge_3	Nb 5.000 Ge 0.077	867 ± 2	Constant η = -39 mV	Nb 59.4 - 65.7 Ge 40.6 - 34.3	Nb_3Ge_2 Nb_5Ge_3	----	Very common mixture
Nb_5Ge_3	Nb 5.000 Ge 0.042	707 ± 2	Constant η = -45 mV	Nb 63.5 - 65.4 Ge 36.5 - 34.6	Nb_5Ge_3	----	
Nb_5Ge_3/Nb_3Ge	Nb 5.000 Ge 0.059	816 ± 2	Constant η = -42 mV	Nb 65.2 - 68.8 Ge 34.8 - 31.2	Nb_5Ge_3 and minor Nb_3Ge	----	
Nb_3Ge/Nb	Nb 5.000 Ge 0.150	760	Constant η = -350 mV	Nb > 95 Ge < 5	Nb and minor Nb_3Ge	8.8 - 9.2 9.2 - 9.3	Very short run. Conditions of operation very remote from equilibrium
Nb	Nb 5.000 Ge 0.000	751 ± 2	Constant i = 5 mA/cm^2	Nb ≃ 100.0 Ge ≃ 0.0	Nb	8.8 - 9.2	

TABLE 3. Summary of Attempts to Electrodeposit Nb_3Ge

Number of Experiments	Range of bath Compositions (mol.%)	Range of Operating Temperatures (°C)	Range of Controlling Electrical Signal	Substrates, morphology and Composition of the Deposits(a)	Remarks
29	K_2NbF_7 ~ 5 K_2GeF_6 0.04 - 0.16	700-870	Constant $\eta^\dagger$ (vs.Mo/Nb(IV), Nb(V) ref.), at the base of first wave. -18 to -45 mV	Mo strip substrates. Stable growth coatings of the phases $NbGe_2$, Nb_3Ge_2, and Nb_5Ge_3 both in single phase and phase mixtures.	The phase Nb_3Ge obtained only as a minor component in phase mixture with Nb_5Ge_3. More details of representative examples are given in Table 7.2.
8	K_2NbF_7 80 K_2GeF_6 0.00 - 0.20	750 ± 5	Same as above. const η . -20 to -30 mV	Mo strip substrates. Coatings mostly of the phase Nb_5Ge_3, sometimes as mixtures with the phase Nb_3Ge as a minor component	Quality of coatings is generally inferior to those of the above entry. The first deposit to appear when starting from zero germanium bath concentration, and continuously increased by anodic dissolution, was the phase Nb_5Ge_3
18	K_2NbF_7 ~ 0.2 K_2GeF_6 0.0 - 0.5	705-750	Constant cell voltage. (cathode vs. Ge anode). -60 to -310 mV.	Pt, Ni, and Nb substrates. Nb was exclusively obtained in all these experiments.	Nb chips were placed in the bath. These, and sometimes Nb cathodes, apparently displaced all germanium ions from solution.
12	K_2NbF_7 0.2 - 2.0 K_2GeF_6 ~ 0.2	712-755	Constant cell voltage (cathode vs. Ge anode). +150 to -360 mV.	W, Mo, Cu, and Ni substrates. Thin layers and powders of various Nb-Ge alloys on W and Mo substrates. Diffused alloys with Cu and Ni substrates.	Unstable growth on W and Mo substrates. Ternary alloys with Ni, and Ge diffusion into Cu (Nb left behind). Intermittent contamination with Fe. See Chapter 8 for more details
9	K_2NbF_7 ~ 6.0 K_2GeF_6 0.1 - 0.15	760 ± 5	Constant cell voltage (cathode vs. Ge anode). -200 to -275 mV	Cu and Pt substrates. Diffused alloy coating Cu-Ge, leaving Nb behind, with Cu. Multilayered diffused ternary alloys with Pt.	A thin transient layer containing Nb-Ge alloy underlying Nb coating. Intermittent contamination with Fe. See Chapter 8 for diffused alloys.
17	K_2NbF_7 ~ 6.0 K_2GeF_6 0.05-0.20	745 - 770	Constant η (vs.Mo/Nb(V), Nb(IV) ref.) -280 to -370 mV.	Cu, Nb, W, and Mo substrates. A thin transient layer of Nb-Ge alloy underlying thick Nb coating, plus loose powders and spongy "umbrella" deposits.	Same as above. When the solution was agitated by bubbling, two regions appeared on the cathode. The lower region (close to the end) was coated with Nb. The upper region (close to the melt surface) was covered with thin Nb-Ge alloy coating.
19	K_2NbF_7 ~ 6.0 K_2GeF_6 0.05 - 0.20	750 - 770	η-steps(b) -210/-310 to -420/+20 mV I-steps 100/0 to 500/-900 mA η-sweep(c) -280/-250 to -350/-320 mV	Cu, Ni, and Mo substrates. Thin adherent layer (less than 1 μm) of Nb-Ge alloys, plus loose powders and spongy "umbrella" deposits on Mo substrates. Diffused alloy coatings with Cu	and Ni substrates.

(Composition determined as average of several microprobe analyses, with ± 5% error of the determination.)

of the various alloys during the anodic part of each cycle.

The problem encountered in this study is probably associated with the thermodynamic instability of Nb_3Ge (16). Alloys which are relatively unstable, or slightly stable, are expected to be difficult to prepare under conditions which are close to equilibrium. The use of high deposition potentials, and hence of conditions which depart strongly from equilibrium, will not produce deposits of good morphology (nor, in these experiments, the required phase).

4. Silicon

The electrodeposition of silicon was an important by-product of investigations of the conditions required for deposition of Nb-Si alloys. Electrodeposition of Si may offer some significant advantages over conventional methods, especially for the formation of relatively inexpensive films for applications in solar cells.

Initial experiments, which were briefly described in the semi-annual Technical Report of January 1976 (CMR-76-1) utilized a 5 m/o solution of K_2SiF_6 in a KF-LiF eutectic at 750°C, with a dissolving silicon anode. Silver or tungsten was used as a reference electrode. These experiments led to the first electrodeposition of epitaxial silicon on (111) n-type silicon substrates. The unintentionally doped films were p-type with a resistivity in the range 0·05 - 1·10 Ωcm. Electron microprobe analysis and Auger analysis failed to detect any impurities, although a resistivity in this range corresponds to about 10^{18} carriers/cm^3. A current density of about 10 mA/cm^2 was found to be a limiting value for stable growth.

Electrodeposition of polycrystalline silicon on metal substrates was also performed using the same solution as for epitaxial deposition. Silver, tungsten and molybdenum were used as cathodes. The two latter metals formed thin WSi_2 and $MoSi_2$ alloy coatings, but the rate of deposition at 750°C far exceeded that of diffusion. As in epitaxial growth, the current density was found to have a pronounced effect on the morphology. At 2 mA/cm^2, nucleation occurred with difficulty

and the material deposited in small islands, growing in bunches of fine needles. An improved deposit was obtained by first electroplating at 4 mA/cm^2 for 3 minutes, then at 2 mA/cm^2. The initial period at the higher current density was found to overcome the problem of isolated nucleation so that uniform, adherent coatings could be produced.

Increase in temperature was found to have a beneficial effect on the morphology of the deposit, but the maximum temperature of alkali fluoride-based baths is limited by their volatility. Attempts were, therefore, made to deposit silicon from silicate-based melts at temperatures well above 750°C. Initially a thermodynamic study was undertaken to determine the most appropriate composition for silicon deposition, using the approach outlined by Johnson (17). In the case, for example, of divalent metal orthosilicates $MSiO_3$, the possible overall reactions are

$$MSiO_3 \rightarrow Si\downarrow + MO + O_2\uparrow \qquad (17a)$$

$$2MSiO_3 \rightarrow 2SiC\downarrow + 2MO + O_2\uparrow \qquad (17b)$$

$$2MSiO_3 \rightarrow 2M\downarrow + 2SiO_2 + O_2\uparrow \qquad (17c)$$

Results for a temperature of 1200°K are summarized in Fig. 9. The results are shown in this relatively limited form, without calculations of the deposition potential, since the free energy of formation of the silicates is not always known. The data of Fig. 9 therefore indicate the stability ranges for deposition of the various possible phases. It may be deduced that aluminum, calcium, lithium and magnesium silicates are relatively favorable for silicon deposition, whereas sodium and potassium silicates will yield only the alkali metal. Johnson (17) found that the theoretical product of electrolysis of calcium silicate is silicon throughout the range from 1200 - 2000°K, while magnesium silicate yields silicon in preference to SiO below 1750°K.

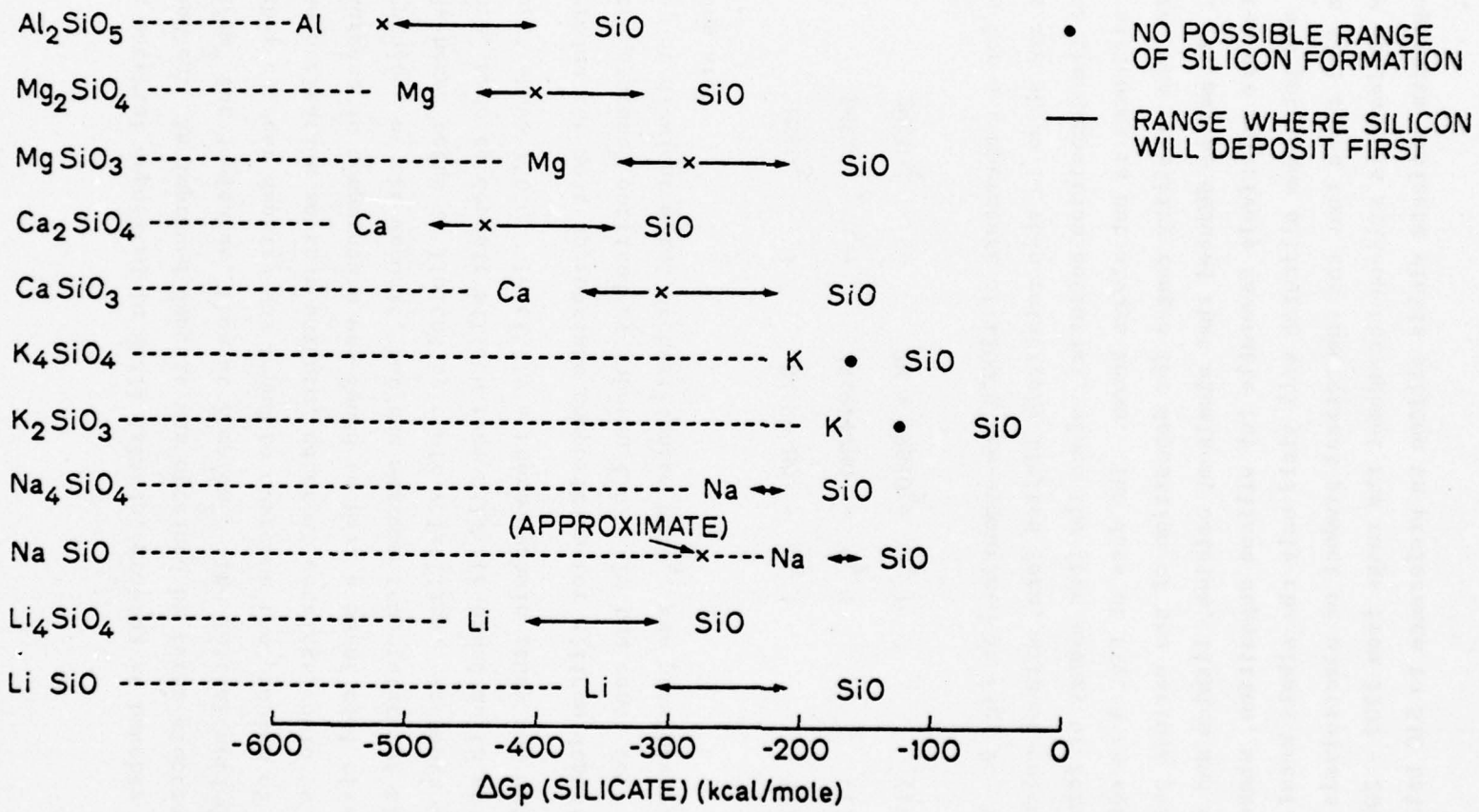

Figure 9. First material to electrodeposit as a function of free energy of formation of silicate at 1200°K. X denotes free energy of formation of silicate where known.

The general conclusion of the thermodynamic study is therefore that the alkaline earth and lithium salts are favorable for electrodeposition of Si. Since the minimum deposition temperature for $MgO-SiO_2$ and $CaO-SiO_2$ based melts would have to be very close to the melting point of Si (1410°), the Li_2O-SiO_2 system was chosen for this investigation. The eutectic, containing 56 w/o SiO_2, melts at 1024°C.

Initial experiments used graphite crucible, graphite anode and graphite cathode. Black deposits were obtained, composed of carbon but with no elemental Si. A molydbenum cathode showed no chemical action with the melt but again no elemental Si was obtained, although microprobe analysis indicated that Si had diffused into the Mo substrate and formed molybdenum silicides. Elemental silicon cathodes reacted with the melt, either by dissolution or by the formation of an alloy of relatively low melting point.

The high viscosity of the silicate melts was considered detrimental to stable growth of Si, and the addition of 5-10 m/o CaF_2 was found to be extremely effective in reducing melt viscosity.

In no experiment was elemental silicon produced, although various silicides could be prepared when, for example, tungsten or niobium were used as cathode in place of molybdenum. It is possible that silicon was deposited at an activity greater than that of these compounds but below that of elemental Si. Very long depositions would be required to equate the silicon activities at the cathode and in the melt.

At the present time, the fluoride-based solvents have been much more successful for electrodeposition of silicon. Further work on this important material appears to be very worthwhile.

5. Gallium Phosphide

Although gallium phosphide was the first compound semiconductor to be electrodeposited (18), the conditions for stable growth of uniform layers had not been previously established.

Gallium phosphide can be synthesized electrochemically from a melt of the composition 75.1 weight % sodium metaphosphate ($NaPO_3$), 7.7 weight % sodium fluoride (NaF) and 17.2 weight % gallium oxide (Ga_2O_3) at temperatures between 750 and 900°C. Gallium phosphide is produced at the cathode of an electrochemical cell according to the reactions:

Cathode:

$$16e^- + Ga_2O_3 + 8PO_3^- \rightarrow 2\,GaP + 3O^{-2} + 6\,PO_4^{-3} \quad \text{or}$$
$$16e^- + Ga_2O_3 + 2PO_3^- \rightarrow 2\,GaP + 9O^{-2} \qquad (18a)$$

Anode:

$$2O^{-2} \rightarrow O_2 + 4e^- \quad \text{or}$$
$$2\,PO_4^{-3} \rightarrow 2PO_2^- + 2O_2 + 4e^- \qquad (18b)$$

Three different substrate materials were studied: 1) graphite which was obtained from Ultracarbon, 2) silicon wafers ((100), n-type, phosphorous doped, 0.3 ohm-cm) which were obtained polished on one side from Siltec and 3) gallium phosphide wafers (111), n-type, sulfur doped, 0.05 ohm-cm) which were obtained from Alusuisse and polished in house. All substrates were surface cleaned with acetone followed by a methyl alcohol rinse before use.

The first experiments were performed on graphite substrates at 900°C. The purpose of these deposits was to confirm that GaP could be deposited from this system. From I-V plots, the minimum deposition potential was found to be ~ 0.6 V. Under all conditions studied, the GaP deposited as needles with some small crystallites present. By varying the time of deposition, it was found that the needle-like growth occurred during the initial stages of growth (<< 1 hr.) and that the small crystallites formed at a later time. This result would be consistent with multiple nucleation at sites with high electric field and the subsequent growth of dendrites. These dendrites would then terminate in the formation of small crystallites.

Because of its availability and close lattice match to GaP, silicon was chosen as a substrate material for early studies. The deposition temperature was 900°C and the minimum deposition potential was found to be ~ 0.5V. Figure 10 shows a comparison between a layer deposited at 20 mA/cm^2 and a GaP layer on silicon grown by organo-metallic chemical vapor deposition. While the electrodeposited layer shows a higher nucleation density, the general morphology of the surface features of the two deposits is similar. The epitaxial nature of the layer was shown by a back reflection Laue photograph of an electrodeposited GaP layer on (100) Si after the silicon substrate had been etched away with HNO_3-HF. More extensive epitaxial deposition was not carried out on silicon since the differential thermal expansion between silicon and GaP is large. The use of silicon substrates is also limited by a chemical reaction with the melt, resulting in "islands" of SiO_2.

The epitaxial growth of GaP on melt-grown GaP wafers was the major system of interest in this study. Initial depositions were at 900°C and at voltages which exceeded the experimentally determined minimum deposition potential of 0.86 volts. Examination of the early deposits indicated that the substrates were etched in the apparatus before deposition. Lowering the temperature to 800°C reduced the amount of etching and raised the minimum deposition potential to 1.16 volts.

A series of depositions over a fixed time of 20 minutes was performed at fixed current densities ranging from 6 mA/cm^2 to 48 mA/cm^2. The results are shown in Fig. 11. The cross sections of the two lowest current density layers (right side Fig. 11) show the formation of coherent layers. However, even at 12 mA/cm^2, some initial formation of surface "craters" was apparent. When the current density was 48 mA/cm^2 the deposit was mostly dendritic. In order to more thoroughly understand this effect, a current versus overpotential (I vs. η) plot was taken using a GaP reference electrode. Figure 12 shows this plot for the cathodic or deposition region. This curve consists of: (1) a linear initial region, (2) a transition region and (3) a second

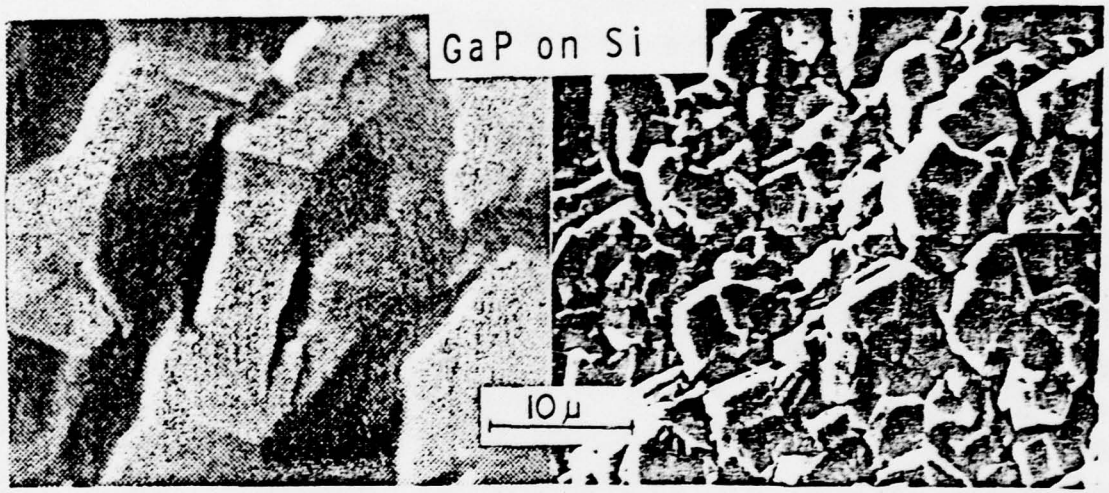

Figure 10. Electrodeposited GaP on Si substrates (right) compared with vapor-deposited layer of J. P. André, J. Hallais, C. Schiller, Journal of Crystal Growth, 31, (1975) 147.

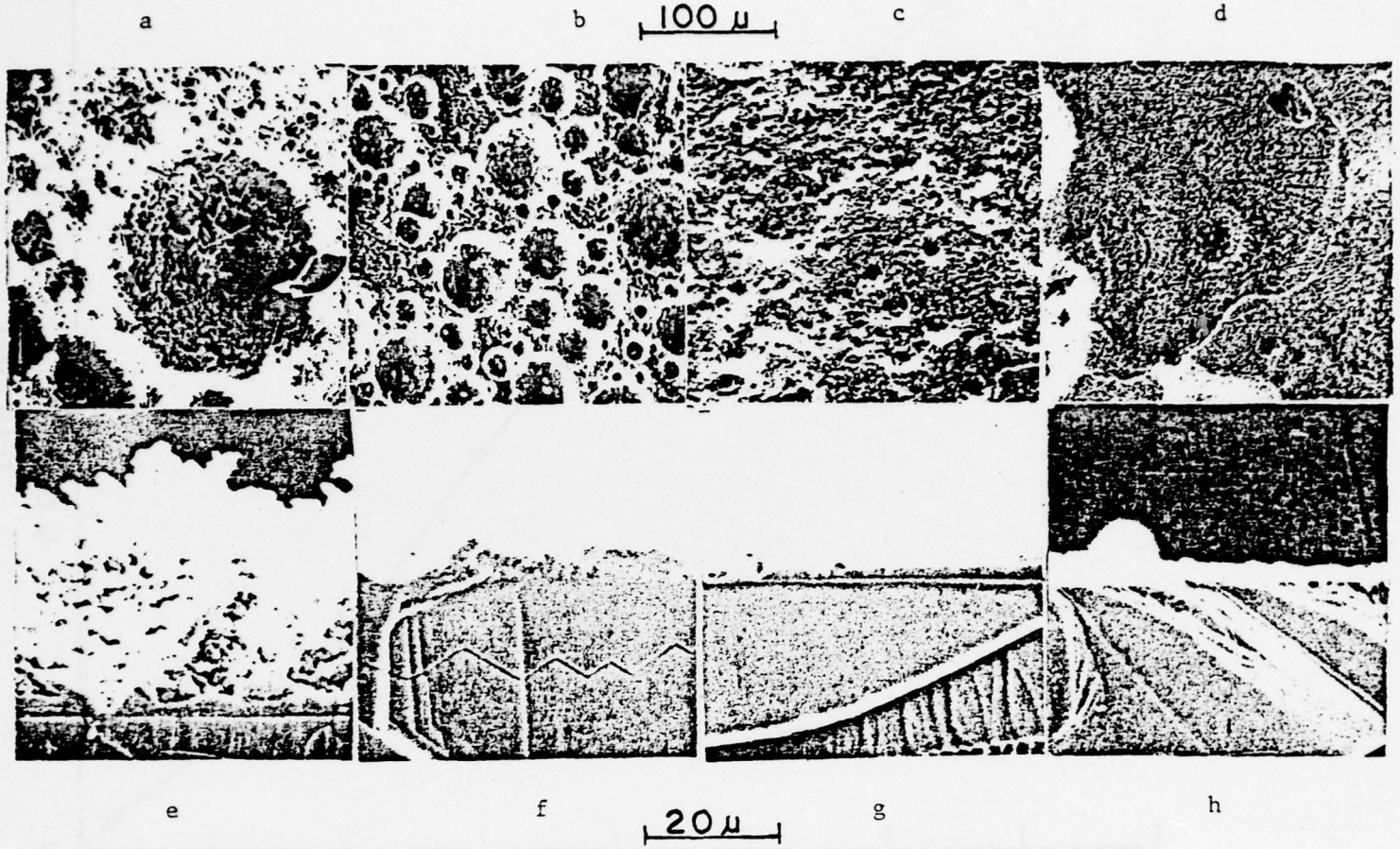

Figure 11. Epitaxial GaP layers on GaP: Upper photographs - normal to layer; Lower - cross section. The current density decreases from left to right: (a) 48 mA/cm^2 (b) 24 mA/cm^2 (c) 12mA/cm^2 (d) 6 mA/cm^2.

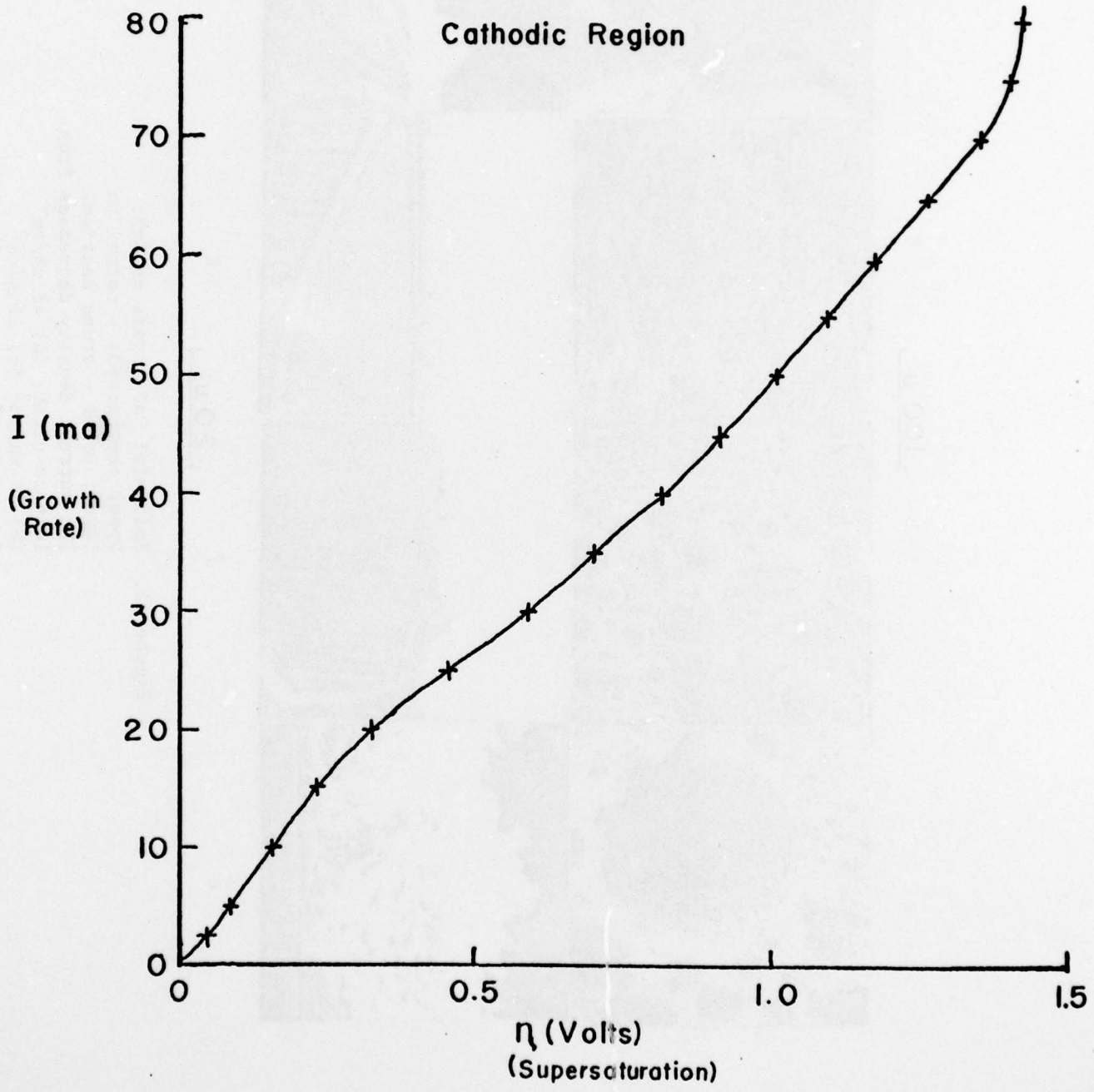

Figure 12. Current versus overpotential during deposition of GaP.

linear region. According to the considerations outlined in Section B.3, these regions may be interpreted as (1) a volume diffusion-controlled region, (2) a transition from volume diffusion control to a dendritic growth region, and (3) a volume diffusion controlled region with a dendritic surface. The results of these experiments indicated that 40 mA/cm^2 was the maximum current density that could be used to produce coherent layers. Figure 13 shows two layers produced under optimum conditions (800°C at 10 mA/cm^2). The layer on the left was deposited in 20 minutes while the one on the right was deposited in 3 hours. The surface features on the long term deposit are very similar to those on GaAs grown by liquid phase epitaxy on (111) substrates.

The parameter which was of chief interest during this investigation was the growth rate which is related to the current density. Variation of this parameter can cause the growth regime to change from that which produces a uniform coherent layer to a dendritic regime. An upper limit on current density appears to be 40 mA/cm^2, but even below this value adverse changes in the surface morphology appear. These changes are related to the evolution of excess phosphorus at the electrode surface: this effect limits the maximum stable growth rate to less than 23 μ/hr (20 mA/cm^2). It is possible that this value could be increased by lowering the P:Ga ratio in the melt, or by substrate rotation.

6. Gallium Arsenide

Molten salt electrodeposition of gallium arsenide was achieved for the first time. The first approach to this problem involved replacement of $NaPO_3$ in the melt used for gallium phosphide deposition by sodium meta-arsenate $NaAsO_3$. This approach was unsuccessful, however, since the meta-arsenate is easily reduced with conversion of As^{5+} to As^{3+} or even As^{o}, in the presence of either carbon, metals or GaAs. Melts based on As_2O_3 or sodium arsenite ($NaAsO_2$) are more stable but are very volatile at the temperatures used for electrodeposition of GaP. Weiss (19) reported the synthesis of molybdenum arsenide MoAs from melts containing $NaAsO_2$ with sodium tetraborate $Na_4B_4O_7$ and NaF.

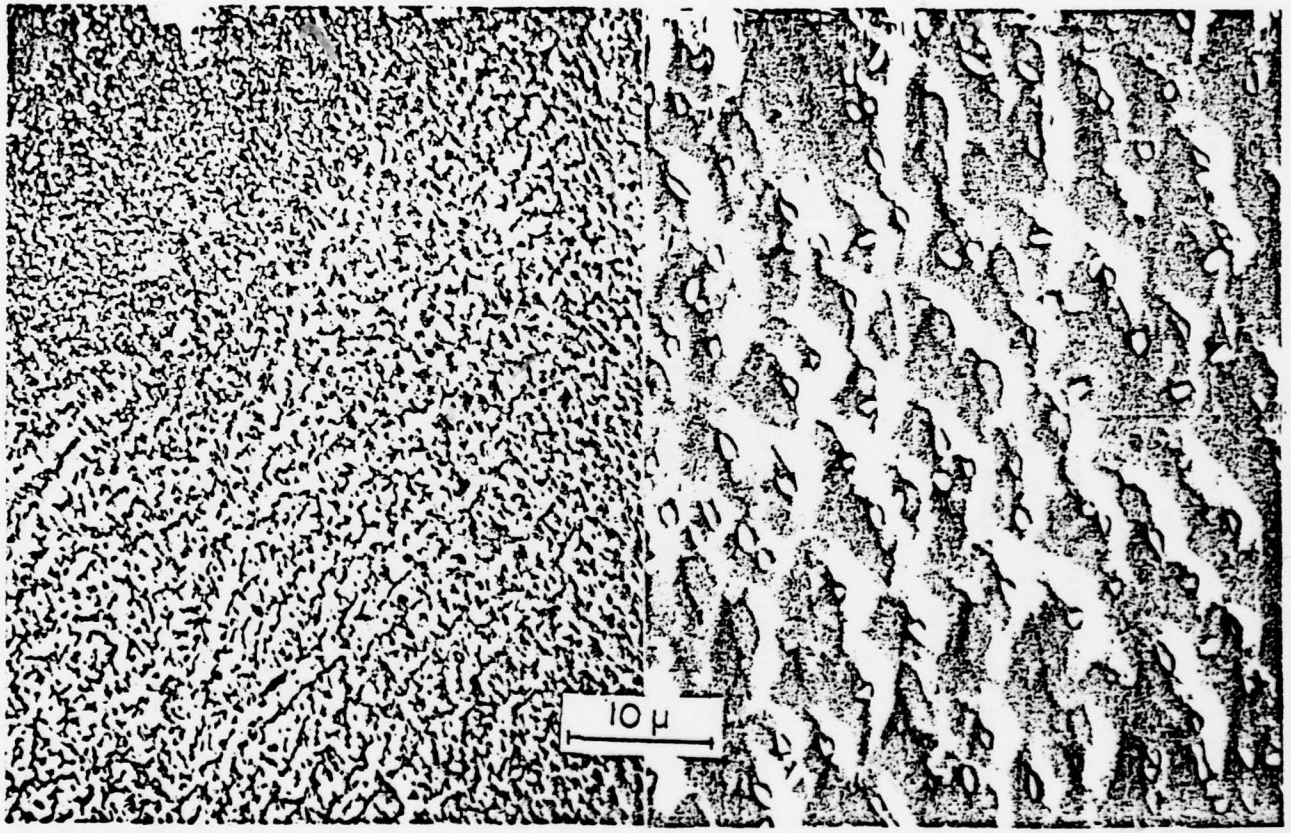

Figure 13. Epitaxial layers of GaP on GaP at 10 mA/cm^2 after 20 mins. and 3 hrs. respectively.

The tetraborate reduces the liquidus temperature of the melt and therefore reduces the rate of evaporation of the $NaAsO_2$ at temperatures where electrolysis may proceed.

In this study, the liquidus temperature was reduced even further by the replacement of the metaborate by boron trioxide B_2O_3. The melt composition which has given the best results to date is 67·4 w/o B_2O_3, 20·3 w/o NaF, 4·2 w/o Ga_2O_3 and 8·1 w/o $NaAsO_2$. The molar concentrations of $NaAsO_2$ and Ga_2O_3 are 4·1% and 1·4% respectively, the excess arsenic being required for deposition of GaAs alone. The minimum deposition potential is 1·7V on GaAs and 2·4V on nickel and a temperature in the range from 720° to 760°C was found to be appropriate. Attempts to deposit GaAs from solutions of Ga_2O_3 and $NaAsO_2$ in a $Li_2O/B_2O_3/LiF$ solvent, which was used to grow LaB_6, were not successful.

The apparatus used in these experiments was similar to that described in our earlier technical reports. Because of the high reactivity of the melt, vitreous carbon crucibles and gold anodes were used. The cathodic substrates were clamped in a carbon holder which did not itself contact the melt.

Identification of the material deposited on the cathode was achieved by several methods. Figure 14 compares the X-ray diffraction data from the deposited material and powdered single crystal GaAs. There is one-to-one correspondence between the peaks (to within 0·1°) except for the appearance of two impurity peaks in the electrodeposited material. These peaks probably arise from the presence of nickel, a major impurity in the deposit, which probably originates from the nickel substrate.

Epitaxial GaAs layers some 10 μm in thickness were electrodeposited on single crystal GaAs substrates. The morphology of these layers does not as yet correspond to that obtained by slow cooling of solutions of GaAs in excess gallium. Further studies to optimize the melt composition and deposition parameters and to reduce impurity incorporation should produce layers whose electrical properties may be studied.

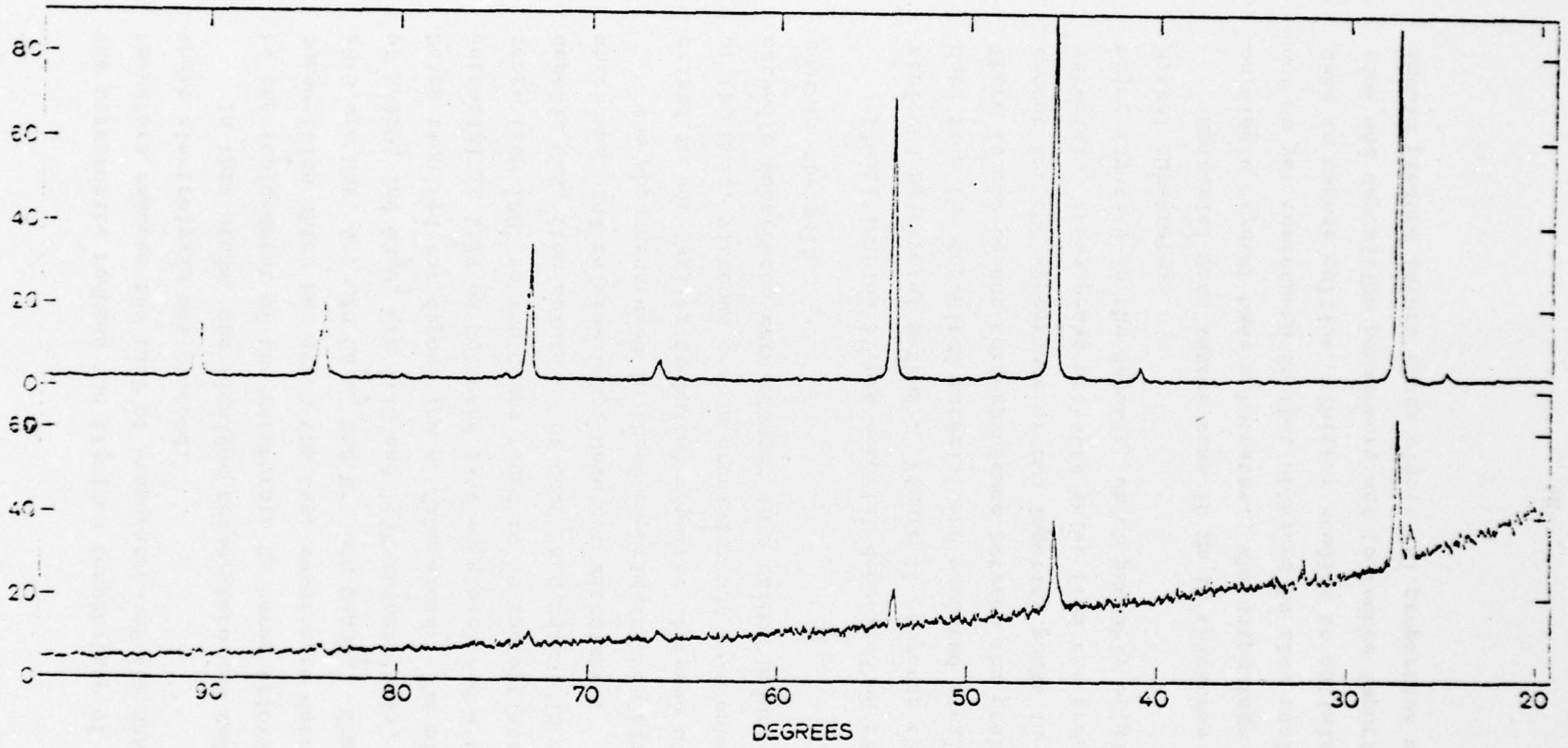

Figure 14. X-ray diffractometer traces of electrodeposited GaAs (lower) and powdered melt-grown GaAs (upper).

7. III-V Semiconductor Solid Solutions

Preliminary attempts were made to deposit solid solutions in the systems $Ga_{1-x}Al_xP$, $GaAs_{1-x}P_x$ and $Ga_{1-x}In_xP$. The $Ga_{1-x}Al_xP$ system was used for the initial study because of its commercial importance in solid state lasers and also because Cuomo and Gambino (18) had reported that AlP could be obtained from a metaphosphate melt by replacing Ga_2O_3 by Al_2O_3. However, when 50% of the Ga_2O_3 in the melt used for GaP electrodeposition was replaced by Al_2O_3, the solubility of the latter at 900°C was found to be negligibly small and only GaP was deposited. Aluminum fluoride AlF_3 was tried in place of the oxide but in a small number of experiments it was not found possible to deposit aluminum either alone or with gallium or phosphorus.

In the case of $Ga_{1-x}In_xP$, the solvent used was an $NaPO_3/KPO_3/NaF/KF$ quaternary eutectic which has been introduced for InP electrodeposition because of the relatively high volatility of In_2O_3. In this case InP was found to deposit in preference to GaP, and no gallium could be detected by electron microprobe analysis in the deposit even when the Ga:In ratio in the melt was 3:1.

The starting composition for the electrodeposition of $GaAs_{1-x}P_x$ was that described in Section D5 with 50% of the $NaPO_3$ replaced by $NaAsO_2$. The melt was contained in a glassy carbon crucible which apparently remained unattacked throughout the experiments. The resulting deposits at 750°C on a nickel cathode with a gold anode were rich in arsenic with no detectable phosphorus. The excess arsenic was probably present as nickel arsenide. Increasing the $NaPO_3$ and Ga_2O_3, together with an increase in the concentration of NaF in the melt to increase the solubility of Ga_2O_3, led to codeposition of Ga, As and P, but the reactivity of the two latter elements with nickel cathodes resulted in multi-phase deposits.

In later experiments, GaAs and GaP wafers were used as cathode, with a deposition potential in the region of 1·7V. Gold was used as the anode. It was found that GaP could be deposited alone, even on GaAs substrates, but changing the melt composition over wide ranges did not yield the solid solution. In the final series of experiments, a melt of composition 52·0 w/o $NaPO_3$, 14·8 w/o $NaAsO_2$, 11·9 w/o Ga_2O_3

and 9·4 w/o NaF was electrolyzed at around 720°C, using a potential of 2·9 or 3·0V and currents of 5-36 mA. On both GaAs and GaP substrates, the deposits consisted of a mixture of GaP and GaAs in a ratio of about 3:1. There was little or no evidence of solid solution formation, which is a very unusual result in view of the absence of a miscibility gap and the relative ease with which solid solutions form by other techniques. The reason for the absence of solid solution formation in the case of these experiments is unknown and it is unfortunate that this problem presented itself at the final stage of this investigation, since it would be of interest to seek a solution.

References

1. A. Wold and D. Bellavance, Preparative Methods in Solid State Chemistry, Ed. P. Hagenmuller (Academic Press, N. Y.) 1972, p. 279.
2. W. A. Tiller, K. A. Jackson, J. W. Rutter and B. Chalmers, Acta Met. 1 (1953) 428.
3. H. J. Scheel and D. Elwell, J. Electrochem. Soc. 120 (1973) 818.
4. R. A. Huggins and D. Elwell, J. Crystal Growth, 37 (1977) 159.
5. R. C. De Mattei, R. A. Huggins and R. S. Feigelson, J. Crystal Growth, 34 (1976) 1.
6. J. P. Randin, J. Electrochem. Soc. 120 (1973) 1325.
7. U. Cohen and R. A. Huggins, "High Rate Electrodeposition of Niobium from Molten Fluorides Using Alternating Square Wave Pulses," presented at meeting of the Electrochemical Society, Dallas, Texas, Oct. 5-10, 1975.
8. T. H. U. Setty and H. Wilmar, Trans Faraday Soc. 51 (1955) 984.
9. A. R. Despic and K. I. Popov, "Transport-Controlled Deposition and Dissolution of Metals," in Modern Aspects of Electrochemistry No. 7 (1972).
10. A. R. Despic et al, J. Electrochem. Soc. 115 (1968) 507.
11. J. W. Diggle et al, J. Electrochem. Soc. 116 (1969) 1503.
12. W. J. Kroll, Trans Electrochem. Soc. 87 (1945) 551.
13. W. K. Burton, N. Cabrera and F. C. Frank, Phil. Trans A243 (1951) 299.
14. V. C. Levich, Russ. J. Phys. Chem. 18 (1944) 335.
15. A. P. Kaputsin, "The Effects of Ultrasound on the Kinetics of Crystallization," Consultants Bureau, N. Y., 1963.
16. T. H. Geballe and A. B. Hallack, private communication.
17. K. E. Johnson, Proc. 3rd Int. Symp. High Temp. Technology (Butterworths, London) 1967, p. 493.
18. J. J. Cuomo and R. J. Gambino, J. Electrochem. Soc. 115 (1968) 755.
19. G. Weiss, Ann. Chim. 1 (1946) 446.

Index of Publications

1. "Surface Structure and Electrolytic Growth Stability of LaB_6 Crystals," D. Elwell, I. V. Zubeck, R. S. Feigelson and R. A. Huggins, J. Crystal Growth 29 (1975) 65.
2. "Silicon Epitaxial Growth by Electrodeposition from Molten Fluorides," U. Cohen and R. A. Huggins, J. Electrochem. Soc. 123 (1976) 381.
3. "DC Resistances in Electrolytic Crystallization from Molten Salts," D. Elwell, R. C. De Mattei, I. V. Zubeck, R. S. Feigelson and R. A. Huggins, J. Crystal Growth 33 (1976) 232.
4. "Crystal Growth by the Electrochemical Czochralski Technique," R. C. De Mattei, R. A. Huggins and R. S. Feigelson, J. Crystal Growth 34 (1976) 1.
5. "LaB_6 Crystals by Molten Salt Electrolysis," I. V. Zubeck, R. S. Feigelson, R. A. Huggins and P. A. Pettit, J. Crystal Growth 34 (1976) 85.
6. "Morphological Stability of a Plane Interface during Electrocrystallization from Molten Salts," R. A. Huggins and D. Elwell, J. Crystal Growth 37 (1977) 159.
7. "Some Prospective Applications of Silicon Electrodeposition from Molten Fluorides to Solar Cell Fabrication," U. Cohen, J. Electronic Mats. 6 (1977) 607.
8. "The Synthesis of GaAs by Molten Salt Electrolysis," R. C. De Mattei, D. Elwell and R. S. Feigelson, J. Crystal Growth (to be published).
9. "Conditions for the Stable Growth of GaP by Molten Salt Electrocrystallization," R. C. De Mattei, D. Elwell and R. S. Feigelson, submitted to J. Crystal Growth.

Index of Technical Reports

Semi-annual	CMR-74-2	July 1, 1973 - Dec. 31, 1973
Annual	CMR-74-6	July 1, 1973 - June 30, 1974
Semi-annual	CMR-75-1	July 1, 1974 - Dec. 31, 1974
Semi-annual	CMR-75-13	June 1, 1974 - May 31, 1975
Semi-annual	CMR-76-1	June 1, 1975 - Dec. 31, 1975
Annual	CMR-77-1	Jan. 1, 1976 - Dec. 31, 1976